Automatic determination of Parting directions, Parting lines and surfaces for two-piece permanent molds

A thesis submitted
In partial fulfillment of the requirements
for the degree of

Master of Technology

by

Pritam Chakraborty

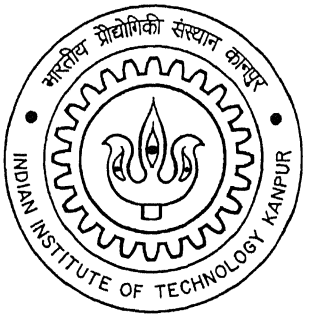

to the

Department of Mechanical Engineering
Indian Institute of Technology Kanpur
Kanpur (India)
July, 2004

CERTIFICATE

It is certified that the work contained in the thesis entitled "***Automatic determination of parting directions, parting lines and surfaces for two piece permanent molds***", by **Mr. Pritam Chakraborty** has been carried out under my supervision and that this work has not been submitted elsewhere for a degree.

Dr. N.V.Reddy
Dept. of Mechanical Engineering
I.I.T. Kanpur

JULY, 2004

Dedicated to my nephew

Riddhiman Banerjee

ACKNOWLEDGEMENTS

I express my deep sense of gratitude and sincere thanks to my thesis supervisor ***Dr. N. Venkata Reddy*** for his excellent guidance, constant encouragement and optimistic outlook, which have been a source of motivation for me throughout this work. I would also like to thank him for his interest and invaluable suggestions during preparation of this document.

I am highly thankful to my Lab. mates, Anupam, Prince, Manas, Kisun, Deepak, Ravi, D.K.Singh Sir, Jaiswal Sir, Sunil Jha Sir and Manufacturing Sc. Lab. staffs, Phoolchand-ji, Verma-ji, Atul, for providing their valuable cooperation and technical help whenever needed. I am thankful to my friends, Ashoke, Abhijit, Somnath, Santanu, Debasis, Raja, Sudhish, Prasad, Kaushik, Anik, Soumya, Raghvendra, Bijoy, Nilesh, Nikhil, Yogesh, Pathak, Padi, Manish, N.R.K, Koustubh, Sandip, Goutam, Siddharta, V.Rakesh, Sutapa, Indrani, Utsa, Kesta, Shamik, Avishek, Shakila, Jayanta and juniors Uttam, Srinivas, Amit, Naga, Danendra, Deep, for making my stay at IIT Kanpur a memorable one.

I am indebted to my parents, Shri Ranjan Kanti Chakrabarti and Smt. Aruna Chakrabarti, my elder brother Roopam Chakrabarty and elder sister Rumpa Banerjee for providing their support without which this journey would have been impossible.

At last, but not the least, I am thankful to everyone who helped me directly or indirectly to complete this work.

Pritam Chakraborty

Contents

List of Figures

List of Tables

Abstract

The mold designing procedure (two piece molds) of a component involves determination of the main parting direction, corresponding side core and cavity directions, parting line generation, gate and runner location/design, cooling channel design and ejection system design. Proper design of molds/dies for a component is necessary to obtain high quality product at lower cost and time. The commercially available CAED systems do not determine the best pair of parting directions, associated side core/cavity directions and parting line of a component and it is still largely dependent on heuristics. This increases the time and cost of production of the dies/molds and even may not guarantee the best design. To overcome the above mentioned problems there is the need to develop a system to automate this procedure.

Review of the literature reveals that there had been few attempts to develop a system that automatically determines the best parting direction, associated best parting line and side core/cavity directions. In most of the previous attempts the parting direction having minimum volume/surface area/number of undercuts is identified as the best parting direction. Other major factors such as flatness of parting line or draw-depth were not considered. Also, parting line along a draw direction is generated by considering the common edges of core and cavity regions. This may not yield the best parting line along a parting direction.

In the present work an attempt has been made to design and develop a system which will automatically determine the best pair of parting direction, corresponding side core and cavity directions, the best parting lines along the candidate draw directions and parting surface along the best pair of parting direction of a component by taking its STL file as input. The cumulative influence of surface area and number of undercuts, flatness of parting line and draw depth is considered as the major factors while determining the best parting direction. A methodology to obtain the best parting line along a draw direction is also developed and implemented. The developed system is validated with the available literature and few case studies are performed to demonstrate its capabilities.

Chapter I

Introduction and Literature Review

1.1 Introduction

Mold and die making is an important industry since their related products represent more than 70% of the non-standard components in consumer products [Fu et al., 1999]. Proper design of molds/dies for a component is necessary to obtain high quality product at lower cost and time. The mold design procedure of a component (two piece molds), involves determination of the main parting directions, corresponding side core and cavity directions, gate and runner location/design, cooling channel design, ejection system design. The high demand for shorter designing and manufacturing lead times of Dies and Molds necessitates automation of the mold designing procedure. The commercially available CAED systems (e.g. Moldflow for injection molding) typically can (i) predict flow front progression and weld line locations, (ii) optimize part wall thickness and process conditions such as injection time, injection temperature, packing pressure, cycle time, (iii) determine injection pressure and clamp forces, (iv) design the cooling systems, (v) estimate warpage for a component [http//:moldflow.com]. However the determination of best pair of parting directions and the associated side core/cavity directions of a component is still largely dependent on the experience of the mold designer. The development of a system devoted in automating this procedure can help in eliminating the heuristics and can reduce time and cost of production.

The *objective* of this thesis work is to design and develop a system which will automatically determine the best pair of parting direction, corresponding side core and cavity directions, parting line and parting surface of a component by taking STL file as an input. There have been many attempts to automate some of the above mentioned aspects but they have some limitations which are discussed later in this chapter. A basic understanding of the molding procedure involving two piece molds is given, prior to the discussion of the published literature.

1.1.1 Basic Concepts

In injection molding and die casting, the molds/dies consist of two plates which form an impression into which molten/ semi molten material is injected. The two plates are known as core and cavity or movable die/mold and stationary die/mold as shown in figure 1.1.

Parting Surface: The contact surface of the two plates in closed position (Fig 1.1).

Parting line: The boundary of separation of the two mold halves in closed position (Fig 1.1).

Parting Directions: The pair of opposite directions along which the two plates of the mold/die separate without obstruction, for removal of the solidified component (Fig 1.1).

Undercuts: Recesses or protrusions on the molded component that prevents its removal along the parting directions (Fig 1.2).

Demoldability: The ability of a component to clear out of the mold core and cavity when the mold opens.

Draw: The minimum distance through which a component is linearly translated in order to clear it from the mold (Fig 1.3).

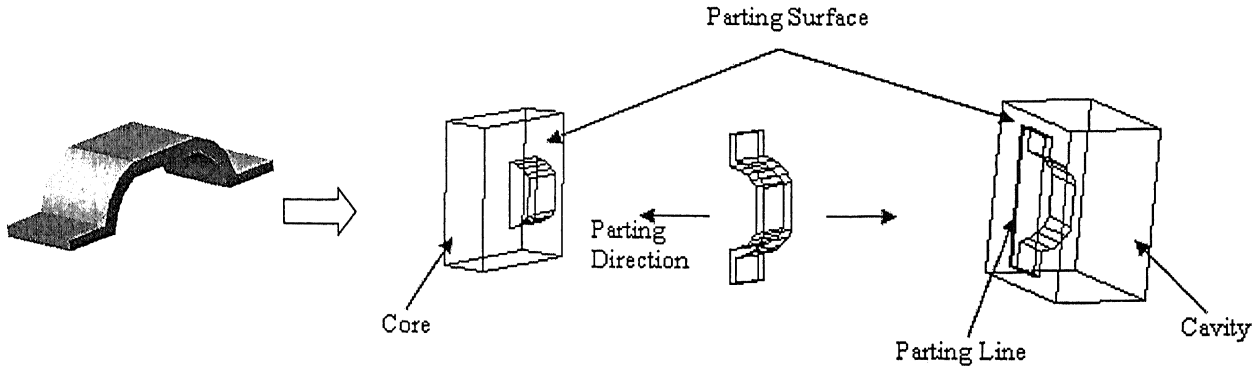

Figure 1.1: A typical part and its mold halves

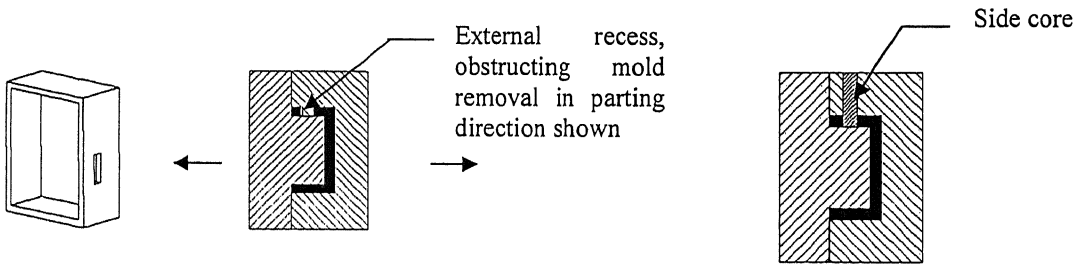

Figure 1.2: A typical part that requires a side core

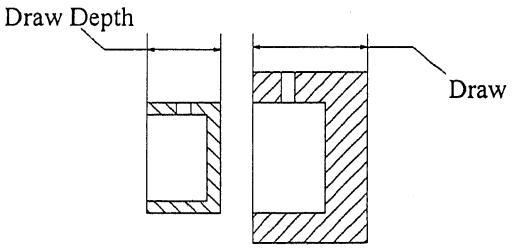

Figure 1.3: Part showing draw and draw depth

1.2 Literature Review

Ravi and Srinivasan [1990] proposed a list of nine decision criteria (projected area, flatness, draw, draft, undercuts, dimensional stability, flash, location of surfaces to be machined) to obtain the

best parting surface once the parting direction has been decided. However these criteria can be applied during the determination of the optimal parting direction itself. Among the above mentioned criteria ***minimization*** *of* number (Weinstein and Manoochehri,1997) *or* surface area (Chen et al.,1993, Hui and Tan, 1992) or volume (Yin et al.,2003, Nee et al.,1997) *of undercut, flatness of parting line* (Weinstein and Manoochehri,1997, Ravi and Srinivasan,1990, Majhi et al.,1999), ***minimization*** *of depth of draw* (Hui and Tan, 1992, Weinstein and Manoochehri,1997) and *draft* (Weinstein and Manoochehri,1997) are considered in determining the parting direction.

1.2.1 Undercuts

In the presence of undercuts, different mold elements such as side cores and cavities are used for easy separation of mold/die halves. However the presence of side core and cavities increases the cycle time and cost of the component. Thus there is the requirement of finding such a pair of parting direction along which there are minimum number and volume of undercuts.

According to Ravi and Srinivasan [1990] the optimal parting plane along a parting direction should be designed to have minimal volume of undercut. This is expressed by equation 1.1.

$$\text{Minimize} \quad F = \frac{1}{V}\sum_i P(F_i)\,|h(F_i) - h(S_k)| \tag{1.1}$$

where F_i is an undercut face, S_k is the parting surface or an intermediate face nearest to F_i, and V is the volume of the solid. However the methodology to obtain the best pair of parting direction is not addressed by them.

Hui and Tan [1992] proposed a method based on heuristic search technique for automating the process of selection of parting direction. A set of parting directions is generated and presence of undercuts along these directions is tested. This set consists of (i) normals of the planar bounding surfaces, (ii) special directions for non-planar bounding surfaces, of the solid. For example in case of cylindrical surface, its axis is considered as a potential parting direction. To check for obstruction, points on the edges of the solid are used. Semi infinite ray that originate from a test point (p_{tp}) is casted along the parting direction under evaluation and is intersected with the enclosing box of the solid as shown in figure 1.4. The line segment is then divided into number of points (p_i) and *Point Membership Classification* (PMC) test of these points (p_i) against the solid is done to check whether a point (p_i) lies *in*, *on* or *out* of the solid. If the PMC test of any of the p_i points is *in*, the corresponding p_{tp} point is obstructed by the solid. They defined a factor called blocking factor to determine the extent of blockage along a probable parting direction and is given by equation 1.2.

$$\textit{Blocking factor (BF)} = \frac{\text{number of obscured points}}{\text{total number of test points}} \tag{1.2}$$

The value of *BF* is calculated for all pre selected parting directions. The pair of direction having the least *BF* is considered as the best pair of parting direction. This methodology is applicable to polyhedral and cylindrical shaped bodies only. Parting direction for complicated solids cannot be obtained by this method. Moreover, optimal parting direction cannot be guaranteed because of the heuristics involved while generating the direction set.

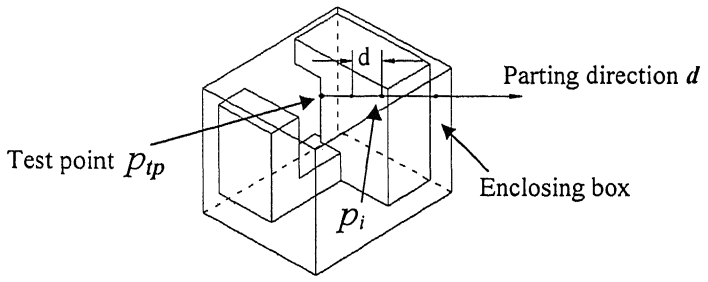

Figure 1.4: Part showing the procedure of blocking used by Hui and Tan [1992]

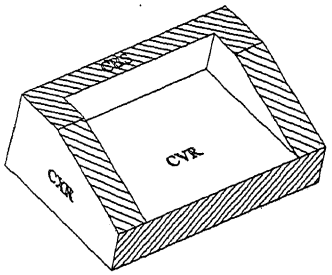

Figure 1.5: Part showing the classification of surfaces (Weinstein and Moonchehri, 1997)

Chen et al. [1993] used the concept of *Visibility Map* (V Map) to obtain the best pair of parting directions for polyhedral object. The *non-convex* regions are first identified from the solid model by using Convex Hull Difference and they are grouped. These are identified as *pockets*. The *Visibility Map* of each pocket is generated. The *Visibility Map* of a pocket is a spherically convex region on the unit sphere. The pair of antipodal points which covered maximum number of *Visibility Maps* of the pockets is considered to be the best pair. The corresponding vectors are selected as the best pair of parting directions.

In the algorithm developed by Weinstein and Moonchehri [1997] the surfaces are classified as convex region surfaces (CXR), concave region surfaces (CVR) and surfaces belonging to concave boundary set (CBS) as shown in figure 1.5. The global concave region contains every surface not assigned to the convex region. The global concave region is divided into individual concave regions, identified as CVR_i. The surfaces within each individual concave region share a common edge with at least one other surface in the same region and are independent of the other CVR_i. The surfaces belonging to CBS are actually convex surfaces adjacent to CVR as shown in figure 1.5. Each

concave region has its own CBS. It is used to subdivide each concave region to calculate its allowable draw direction. The surfaces within each CVR_i are further divided into sets, if their outward normal forms a positive scalar product with the outward normal of a surface within the associated CBS. The allowable draw range of the sub sets in each concave region is first obtained. The allowable draw range of each concave region is then obtained by the union of the allowable draw ranges of the individual sets. The intersection of the allowable draw ranges of each concave region determines the allowable draw range of the part. A null draw range signifies the presence of an undercut. But this methodology can only be applied to polyhedral objects. Moreover in the presence of interacting features, the *pockets* have to be decomposed which affects the global nature of the *Visibility Map* of the pockets and hence the methodology fails.

The algorithm developed by Nee et al. [1997] consists of two major steps. Firstly, all the possible undercuts are recognized and extracted. The undercuts are classified as *outside external undercuts* [Fig 1.6 (b)], *inside external undercuts* [Fig 1.6 (a)], *internal undercuts* [Fig 1.6 (c)]and *curved surface undercuts*. The classification is made based on the relative positions of surfaces surrounding a particular surface or *target surface*. Among the *curved surface undercuts*, cylindrical, conical, spherical, revolved and B surfaces are considered.

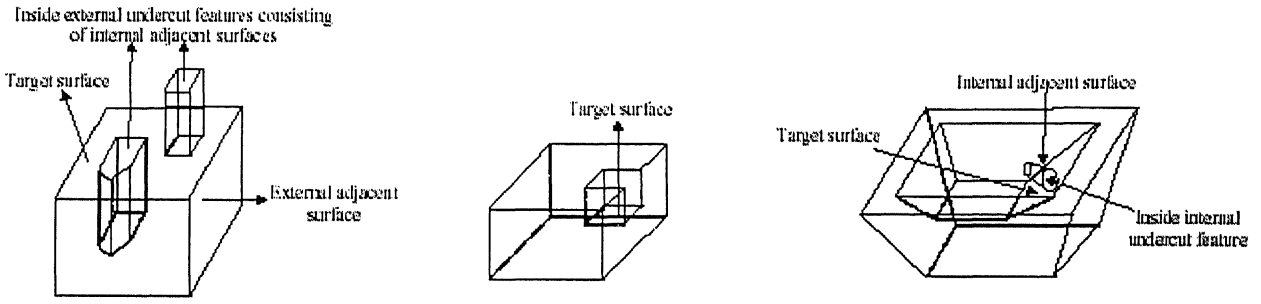

(a) Inside External Undercut features (b)Outside External Undercut features (c)Inside Internal Undercut features

Figure 1.6: Parts showing different types of external features (Nee et al., 1997)

After all the possible undercuts are identified, the corresponding undercut directions are identified based on the rules given in table-1.1. The volume of each undercut is also calculated. A direction list consisting of all possible visible directions selected based on the above mentioned rules is made. Each direction ***d*** in the direction list is tested as probable parting direction. Amongst all the possible undercuts those having undercut direction (visible direction) parallel to ***d*** are grouped. The best parting direction is selected based on the criteria given by equation 1.3.

$$V_{i\max} = \mathrm{Max}[\sum_{j=1}^{m_i} V_{ij}(d)] \qquad (i=1, 2,\ldots n) \qquad (1.3)$$

where ***d*** is the undercut direction, n is the undercut group number and m_i is the undercut number in the *ith* group. Based on the above criterion, the sum of the volumes (V_{imax}) of visible undercuts in the

optimal parting direction should be greater than the ones in any other groups. However the reduction in volume of undercuts along a direction may not guarantee the reduction in the number of undercuts. An increased number of undercuts increases the cycle time and reduces productivity. Thus along with the volume, the number of undercuts should also be taken into consideration.

Types	Three-S_A	Four-S_A	More than four-S_A
Cases	Fig.2(a)	Fig.2(b)	Fig.2(c)
Undercut criteria	(1) $L_k > 0$, $x_{1k} > x_k$, $x_{2k} > x_k$, and $x_{3k} < x_k$ OR $L_k < 0$, $x_{1k} < x_k$, $x_{2k} < x_k$, and $x_{3k} > x_k$. (2) P: Nil	(1) $L_k > 0$, $x_{ji} > x_k$ (j=1,2,3) and $x_{4i} < x_k$ OR $L_k < 0$, $x_{ji} < x_k$ (j=1,2,3) and $x_{4i} > x_k$ (2) P: Nil	(1) V_{j-2}, V_{j-1} and V_j constitute a concave portion and V_{j+1}, V_{j+2} and V_{j+3} form another one (2) P: Nil
Undercut direction	(1) L_i, when $L_i \bullet L_{1i} \geq 0$ and $L_i \bullet L_{2i} \geq 0$. OR (2) $(L_i \times L_{1i} + L_{2i} \times L_i) / \lvert L_i \times L_{1i} + L_{2i} \times L_i \rvert$, when $L_i \bullet L_{1i} < 0$ or $L_i \bullet L_{2i} < 0$.	(1) L_i, when $L_i \bullet L_{ji} \geq 0$ (j=1,2,3). OR (2) $(L_i \times L_{1i} + L_{3i} \times L_i) / \lvert L_i \times L_{1i} + L_{3i} \times L_i \rvert$, when $L_i \bullet L_{1i} < 0$ or $L_i \bullet L_{3i} < 0$.	(1)$(L_{j-1,i}+L_{j-2,i}+L_{j+2,i}+L_{j+1,i}) / \lvert L_{j-1,i} + L_{j-2,i} + L_{j+2,i} + L_{j+1,i} \rvert$, when $L_{ji} \bullet L_{j-1,i} \geq 0$ and $L_{ji} \bullet L_{j+1,i} \geq 0$, OR (2) $(L_{j-1,i} \times L_{j-2,i} + L_{j+2,i} \times L_{j+1,i}) / \lvert L_{j-1,i} \times L_{j-2,i} + L_{j+2,i} \times L_{j+1,i} \rvert$, when $L_{ji} \bullet L_{j-1,i} < 0$ or $L_{ji} \bullet L_{j+1,i} < 0$

Criteria and U_D of outside external undercuts

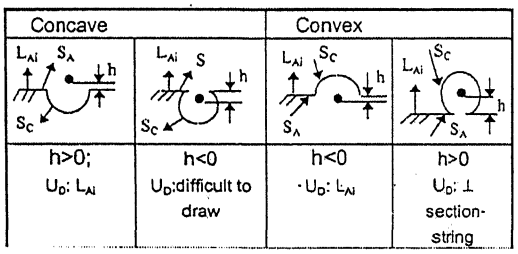

Spherical surface undercuts

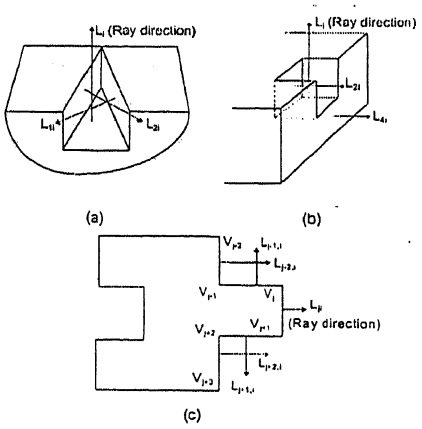

Cases of outside external undercuts

$(L_{1i} \times L_{2i} + L_{3i} \times L_{4i} + \cdots\cdots L_{n-1,i} \times L_{ni}) / \lvert L_{1i} \times L_{2i} + L_{3i} \times L_{4i} + \cdots\cdots L_{n-1,i} \times L_{ni} \rvert$ (If n is an even number)

OR

$(L_{1i} \times L_{2i} + L_{3i} \times L_{4i} + \cdots\cdots L_{n,i} \times L_{1i}) / \lvert L_{1i} \times L_{2i} + L_{3i} \times L_{4i} + \cdots\cdots L_{n,i} \times L_{1i} \rvert$ (If n is an odd number)

U_D of inside external undercuts

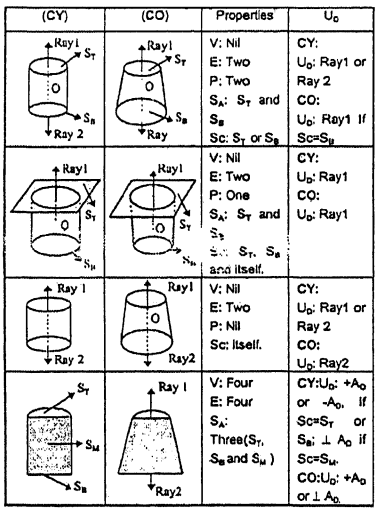

Cylindrical, conical surfaces and their undercuts

Table 1.1: Undercut directions of different types of undercuts developed by Nee et al. [1997].

Hui [1997] extended the algorithm based on heuristics developed by Hui and Tan [1992] to handle objects that can be molded with a 2-piece molds having side cores and/or split cores. They selected a parting direction where the number of split and side cores is minimum. A search space of directions is created consisting of normals to individual faces of the object from which the main directions and corresponding side core directions are selected. The face normals of the openings of the cavity determine a zone of possible directions for clearing the corresponding undercut. Hence additional directions are also considered in the search space. The opening of cavity refers to a face f_{op} of the cavity such that f_{op} is not a face of the solid. In order to take into consideration the existence of recesses, an unit vector in the direction of $n \times n_{op} \times n$ which is the projection of $\mathbf{n}_{op}$ onto a face f with face normal $\mathbf{n}$, is included in the search space. Although this methodology can handle split cores but it is incapable of handling complicated and arbitrary shaped components.

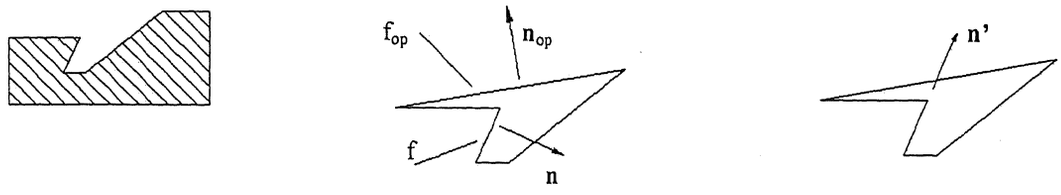

Figure 1.7: The additional directions as developed by Hui [1997]

Ying et al. [2001] developed a methodology using *freedom cones* (FCs) and *non-directional blocking graph* (NDBG) to generate optimal pair of parting directions. The *freedom cone* consists of the directions along which a potential undercut feature can translate without obstruction. Regularized difference between the part and its convex hull is performed to identify the potential undercut features or *maximal connected components* (MCCs) as shown in figure 1.8. If the *freedom cone* of a maximal connected component is non-zero it is recognized as *isolated potential undercut feature* (ISPUF) else it is an *interacting potential undercut feature* (INPUF). The INPUF is recognized by decomposing it into convex cells and reconstructing them by systematically connecting the small cells using NDBG. The global freedom cone of the MCC is same as the local freedom cone because the moving directions of an MCC are constrained only by the contacting faces of the MCC with the part. A list of all the MCCs is prepared. Non-directional Blocking Graph (NDBG) of the MCCs is used to obtain the parting directions. The optimal parting direction is one along which maximum number of potential undercut features can be retrieved without collision. However the approach is

inefficient in handling complicated objects with freeform surfaces where the contacting faces of the MCCs are difficult to obtain.

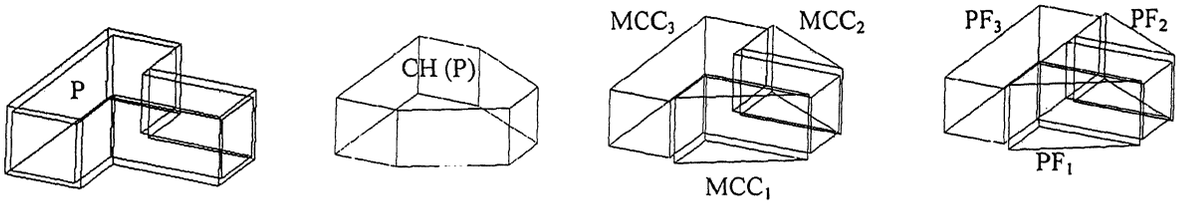

Figure 1.8: Example of maximal connected components (Yin et al. [2001]).

Priyadarshi et al. [2004] developed a methodology to select candidate parting directions for multi-piece molds. A set of directions favorable to be candidate parting directions are (i) directions associated with coordinate system (ii) planar face normals (iii) cylindrical/conical face axis. This set is generated based on heuristics. The direction set is further expanded by triangulating the surfaces and considering facet normal directions. The triangulated facets are partitioned into a collection of disjoint sets. A set of accessible facets along each candidate parting direction is determined. The accessibility test along the directions is performed by *separating axis condition* [see Appendix C]. Near optimal mold piece are selected from the set of directions and corresponding accessible facets by treating it as a set cover problem. However, the set of directions used to perform accessibility test may not be sufficient to extract features such as a depression generated by using NURB surfaces.

All the above works uses first feature recognition and then the visibility of features to determine the pair of parting directions. The procedure used for feature recognition and visibility of feature differ from one to the other. The broad classification of the above attempts is shown in figure 1.9.

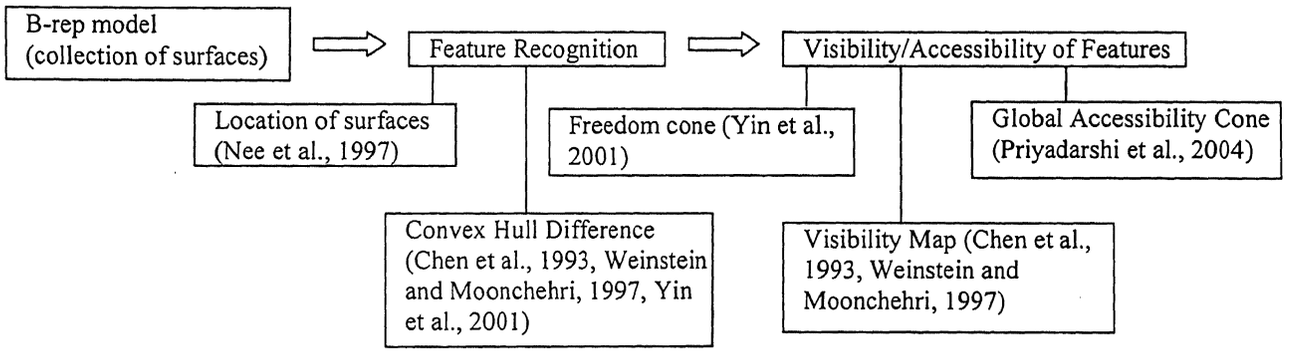

Figure 1.9: Classification of methodology as used by different authors

It is noticeable that accessibility/visibility of the non convex regions plays a pivotal role while assessing the demoldability of a component along a pair of parting direction. Freedom cones, Visibility map and Accessibility cones gives a measure of accessibility of surfaces. However global

accessibility cones are more efficient when demoldability of complicated components involving free form surfaces and interacting features is to be obtained.

1.2.1.1 Analogy between Visibility and Demoldability

A part is *completely visible* (demoldable) along a pair of direction if all the surfaces comprising the part are visible along that pair of direction. A surface **S** on an object **Ω** is completely visible in one viewing direction ***d*** if for every point **p** on **S**, the ray starting from infinity to **p** in the direction ***d*** does not intersect the interior of **Ω** as shown in figure 1.10. *Partial visibility* is guaranteed if for at least one point **p** on **S** the ray starting from infinity to **p** in the direction ***d*** does not intersect the interior of **Ω** [Chen et al., 1993]. A direct analogy between demoldability and visibility can be made because when a surface **S** is removed from the mold/die along a parting direction ***d***, the trajectory of each point on **S** forms a ray from the point to infinity in the direction ***d***. Since demoldability of a part involves both the core and cavity, hence visibility has to be ensured along the pair of direction $+d$ and $-d$ to estimate its demoldability. *Undercuts* are those regions or surfaces on the object **Ω** which are invisible along $+d$ and $-d$ directions.

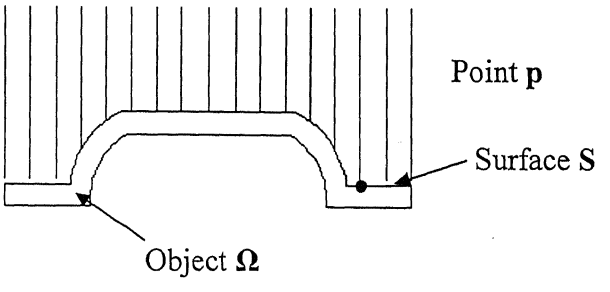

Figure 1.10: Part showing complete visibility

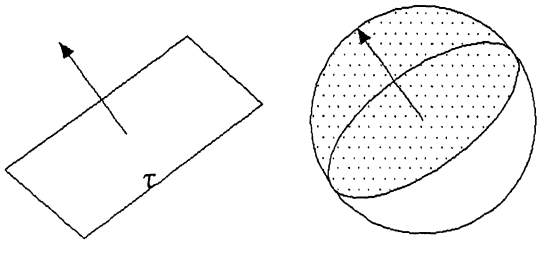

Figure 1.11: Example of a plane surface and its Visibility Map

1.2.1.2 Visibility Map and Global Accessibility Cones

Any point p (on a surface) having normal η and tangent plane τ is visible from all the directions up to a hemisphere with η being at the North Pole and τ being the equatorial plane. The visibility of a surface is estimated by the intersection of all the hemispheres of the points constituting the surface. The resulting spherically convex region is called the Visibility Map (V Map) of the surface. Any point in the VMap corresponds to a direction from which the entire surface is locally visible [Chen et al., 1993]. A plane surface and its corresponding VMap is shown in figure 1.11. For non-planar surfaces, instead of considering discrete points on the surface, it can be subdivided into convex planar regions and intersection of the VMaps of these planar regions guarantees the local visibility of the surface. However VMap do not guarantee global visibility/accessibility in the presence of interacting features.

Dhaliwal et al. [2002] developed a methodology based on **global accessibility cone** which uses the basic concept of VMap to determine the accessibility of a surface. The procedure involves the discretization of a surface into planar triangular facets. The global inaccessibility region **I** of each facet f due to the presence of other facets f_i is recognized. The total inaccessibility region **I=I** U (interior of f_i^p) where f_i^p is spherical projection of f_i is obtained. The accessibility region **V=H-I** where **H** is the outward hemisphere using outward normal vector of f as the pole is obtained. The inaccessibility region due to the interior of f_i^p is governed by the inaccessibility region of its edges. This makes the procedure computationally efficient. Global accessibility of any form of surface can be guaranteed by this procedure. However triangulation of the surfaces constituting the solid is essential in order to implement this algorithm. Hence usage of STL file of a component is beneficial since a tessellated model consisting of triangular facets and normals is provided in a STL file which makes the process of triangulation redundant.

1.2.2 Parting line/surface

A flat parting surface reduces the time and cost involvement in manufacturing the dies and molds because tight tolerances are not required in the manufacturing of the die/mold halves. A flat parting surface also makes the design of the clamping system easier. Hence a flat parting surface is very much desirable. The evaluation of flatness of parting line gives a direct measure of the flatness of parting surface. Parting line geometry depends on the parting direction chosen and is another important criterion while determining the best pair of parting direction. A parting direction yielding a flat parting surface is preferred over one yielding an uneven parting surface.

Ravi and Srinivasan [1990] defined a factor F (equation 1.4) to estimate the degree of flatness of parting surface along a defined parting direction.

$$F = A(Q \cap PS_i) / P(Q \cap PS_i) \quad (1.4)$$

where the numerator is the intersection of the solid with the parting surface and the denominator is the projected area of the parting surface on the view plane normal to the draw vector.

Hui and Tan [1992] used an approach based on sweep operation whereby the mold boxes are generated. However no criterion governing the flatness of parting line/surface is mentioned.

Weinstein and Manoochehri [1996] developed a methodology to obtain parting lines along draw directions having no undercut. The draw range of each non-convex region is first evaluated and the allowable draw range of the part is then obtained by intersecting the allowable draw ranges of the non-convex regions. The V-Map of convex region is then used to generate the parting lines. The parting lines are placed on the edges of the surface to maintain aesthetics of the final product. The major drawback of this methodology is that it can obtain parting lines only along those directions which have no undercut. Moreover, it can only be applied to parts having planar surfaces.

To select the best parting line from a set of parting lines, Weinstein and Manoochehri [1997] defined the *degree of flatness* as root-mean-square (RMS) deviation of the vertices that define the parting line from the best plane that passes among all the vertices. An RMS value of zero indicates that all the vertices lie on the same plane. The RMS distance of each vertex in the parting line from its best-fit plane for the j possible parting line is given in equation 1.5.

$$F_1 = RMS_j = \sqrt{\frac{\sum (p_i - p_i')^2}{n}} \quad (1.5)$$

where p_i is the actual vertex in the selected parting line and p_i' is its perpendicular projection onto the best fit plane.

Majhi et al. [1999] developed two methodologies whereby the flattest and undercut free parting line for a convex polyhedron can be obtained. The first methodology attempts to find a direction d that maximize equation 1.6.

$$\rho(d) = \sum_{i=1}^{k} length(\hat{e}_i)^2 / \sum_{i=1}^{k} length(e_i)^2 \quad (1.6)$$

where e_i's are the line segments constituting the parting line and $\hat{e}_i$'s their projections on a plane perpendicular to d.

The function $\rho(d)$ can be modified to $\rho(d) = \sum_{i=1}^{k} length(\hat{e}_i) / \sum_{i=1}^{k} length(e_i)$. However this makes the optimization problem highly non-linear and hence equation 1.6 is preferred by them. The second method considers the width of the parting line [$\omega(d)$] in direction d as the smallest distance between two parallel planes that are normal to d and enclose the parting line. The objective is to find a

direction ***d*** that minimizes $\omega(d)$. A parting line lying in a plane is most desirable and it is obtained when $\omega(d) = 0$.

Fu et al. [2002] devised an algorithm to obtain the parting line for a given parting direction. Based on the orientation of normal of the surfaces relative to core and cavity directions they can be classified as *potential core molded* or *potential cavity molded* or *dual surfaces*. A dual surface is categorized as core molded if there are more edges neighboring to the potential core molded surfaces than potential cavity molded surfaces and vice versa. If dual surfaces do not have any neighboring relationship the surfaces should not be considered as the core or cavity molded surfaces. The undercut feature surfaces are also extracted. Thus the final core/cavity molded surfaces are core/cavity molded surfaces subtracted by the dual surfaces in undercut features. Parting line is the maximum external edge-loop in the core or cavity molded surfaces. The edges are then extruded to generate the parting surface. However no flatness criterion is proposed.

Yin et al. [2004] defined the flatness of the parting line (FPL) in the parting direction ***d*** as given by equation 1.7.

$$\text{FPL}(d) = 1 - \sum_{i=1}^{k} length(\hat{e}_i)^2 / \sum_{i=1}^{k} length(e_i)^2 \qquad (1.7)$$

where e_i's and $\hat{e}_i$'s similar to Majhi et al. [1999]. The smaller the value of FPL (d), the flattest is the parting line.

1.2.3 Draw depth

From the definition of draw it is clear that an increased draw depth will (i) increase the draft to the vertical surfaces, (ii) increase draw capability and (iii) increase cycle time and reduce productivity. Thus it is essential to choose a parting direction along which the draw depth is kept to a minimum. Hence draw depth forms another important criterion in determining the best pair of parting directions.

Ravi and Srinivasan [1990] included draw and draft in the list of criteria essential while determining the best parting surface. Since draft is dependent on draw depth hence evaluation of draw depth can determine draft. The best parting surface is the one that minimizes equation 1.8.

$$F = \frac{1}{L} \max |h(V_i) - h(PS_i)| \qquad (1.8)$$

where L is the maximum dimension of the solid, $|h(V_i) - h(PS_i)|$ is the distance of each vertex from the parting surface.

Hui and Tan [1992] have not considered draw depth but used shear contact of the mold and mold plate as a criterion in their attempt. A parting direction yielding the least shear contact area is preferred.

Weinstein and Manoochehri [1997], defined draw depth along a parting direction $\boldsymbol{d}$ by $Max|(v_i - v_j).d|$ where v_i are vertices belonging to the part and v_j are vertices belonging to parting line. Yin et al. [2004] used a similar function in their attempt. However in the absence of a flat parting line, exact draw depth will not be obtained by $(v_i - v_j)$.

1.3 Scope and Objective of the Present Work

From the literature review it can be observed that minimizing the number and/or volume and/or surface area of undercuts only will not suffice to obtain the optimal pair of direction in complicated processes such as injection molding and die casting. Other important criteria such as flatness of parting line and minimal draw depth along the parting directions have to be simultaneously taken into consideration. The search space of parting directions has been enhanced in this work by including directions $\vec{d} = \vec{\eta}_i \times \vec{\eta}_j$ with $i \neq j$, where $\vec{\eta}_i$, $\vec{\eta}_j$ are the normals of the facets belonging to a particular isolated non-convex region. The search space of directions used in the earlier attempts is primarily based on heuristics and is not competent enough to handle freeform surfaces with depressions, etc. Moreover V-Map and Freedom cones are not efficient enough to obtain global accessibility for freeform features and features in complicated components. Global accessibility cone however provides an accurate estimation [Dhaliwal et al., 2002]. But tessellation of the surfaces is necessary to implement this concept. Hence STL file is used in the present work which provides a major advantage over B-rep model used in all the previous attempts.

In the present work a system has been developed that considers STL file of the component as an input and identifies the best pair of parting direction, corresponding side core and cavity directions, generates parting line and STL file of parting surface. All the dominant criteria such as minimization of surface area and number of undercuts, parting line/surface flatness and minimization of draw depth has been considered. The optimal parting direction is obtained by considering cumulative contribution of all the factors.

1.4 Organization of the Thesis

Introduction and literature review is done in Chapter 1. The problems associated with the existing procedures are presented. A brief idea about global accessibility cone and its advantage over V Map and Freedom cones has been described. The objective of the present work is also given.

The methodology used to determine parting directions and corresponding side core/cavity directions is presented in Chapter 2. Identification and grouping of non-convex regions forming the probable undercut regions, generation of parting direction list and accessibility analysis along these directions is discussed in detail. Calculation of factors giving a measure of visibility, flatness of

parting line and draw depth for all the parting directions is presented. Selection of an optimal parting direction based on the cumulative influence of all factors considered is defined in this chapter.

The methodology employed to determine the flattest parting line and parting surface for a given parting direction is presented in Chapter 3. The procedure to identify valid non-convex perpendicular regions, constraining non convex non perpendicular regions and undercut regions to obtain the location of parting line is described. The generation of parting line and parting surface is discussed in detail.

The design of the system and the implementation of the methodologies developed in the present work are presented in Chapter 4. The information flow in the different modules of the present system is shown by means of flowchart. The inputs to the system and the outputs from the system are also described.

Few validations and case studies to demonstrate the correctness and capabilities of the present system are presented in Chapter 5.

Conclusions from the present work and scope of future work are presented in Chapter 6.

Chapter II

Determination of Parting and Side Core/Cavity Directions

2.1 Introduction

The best pair of parting direction for a moldable component (using injection molding and die casting) is primarily influenced by factors such as number and/or surface area and/or volume of undercuts, flatness of parting line and draw depth. Determination of optimal parting direction involves the collective influence of these three major factors. The collective influence of the three major factors to obtain the best parting direction for any form of solid object is not considered in any of the previous attempts. In the present work the combined influence of all the three factors mentioned above for any arbitrary shaped component has been considered. The search space of parting directions has been enhanced in this work by including directions $\vec{d} = \vec{\eta}_i \times \vec{\eta}_j$ with $i \neq j$, where $\vec{\eta}_i$, $\vec{\eta}_j$ are the normals of the facets belonging to a particular isolated non convex region. The search space of directions used in the earlier attempts is primarily based on heuristics and is not competent enough to handle freeform surfaces with depressions, etc. An ideal parting direction is one along which the number/surface area of undercuts is minimum, the parting line is the flattest (lie in a plane) and draw depth is minimum. However in pragmatic situations this is difficult to achieve. Hence in such cases a weighted contribution of all the three factors has to be considered.

In this chapter the methodology to identify the probable undercut regions, to obtain the global set of parting directions and the accessibility analysis along the directions is discussed in detail in section 2.2. Flatness of parting line and draw depth calculation along each direction is described in sections 2.3 and 2.4 respectively. The procedure used in incorporating the cumulative influence of the three factors along the parting directions is described in section 2.5. The methodology to obtain the side core and side cavity directions is also presented in section 2.6.

2.2 Minimization of Number and Surface area of Undercuts

Convex regions are accessible over any pair of direction. Only the non-convex regions are prone to obstruction and hence they form the probable undercut regions. As can be observed from literature review (section 1.2.1), that the overall procedure of identification of a parting direction having minimum number and/or surface area and/or volume of undercut consists of two major steps.

Firstly recognition of non-convex regions which form the probable undercut features and secondly the accessibility of these regions along a set of directions to obtain the optimal pair of parting directions having minimum volume/number/surface area of undercut features is carried out. In the present work the above mentioned steps have been followed using the STL file of the component model as an input. The probable undercut regions are identified and a broad classification of the undercut regions is carried out based on mutual concavity of the facets forming these regions and local visibility of these regions.

2.2.1 Identification of Probable Undercut Regions

The non-convex regions form the probable undercut regions. Hence they have to be identified and grouped.

2.2.1.1 Non-Convex Regions

A facet f_k is defined to *be non-convex* if $\vec{\eta}.\frac{\vec{v}_{ij}}{|\vec{v}_{ij}|} > 0$ for i=1 to 3 and j=1 to 3 with any facet f_l where $k \neq l$ in the set $\{F_{total}\}$ of facets bounding the object. Here $\vec{\eta}$ is the normal to a facet whose convexity with respect to other bounding facets is being checked and $\vec{v}_{ij}$ is the vector joining its vertices to any other facet vertices as shown in figure 2.1. The grouping of the non-convex facets is done based on connectivity of the facets. Thus a set $\{F\} = \{F_1, F_2, .. F_N\}$ of separated non-convex regions is obtained as shown in figure 2.2. Each group $\{F_i\}$ is a separate probable undercut region visible over a certain zone defined by its V-Map [Chen et al., 1993]. However, the presence of interacting features as shown in figure 2.5 (b) renders the region invisible. Hence there is a need to separate the interacting regions also.

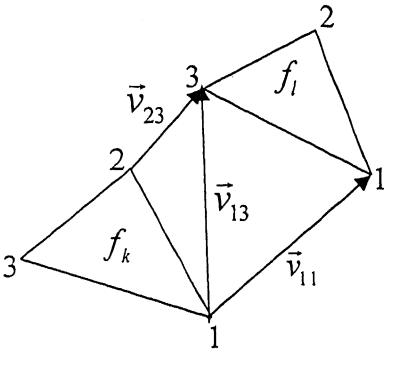

Figure 2.1: A schematic diagram showing convexity testing between two facets

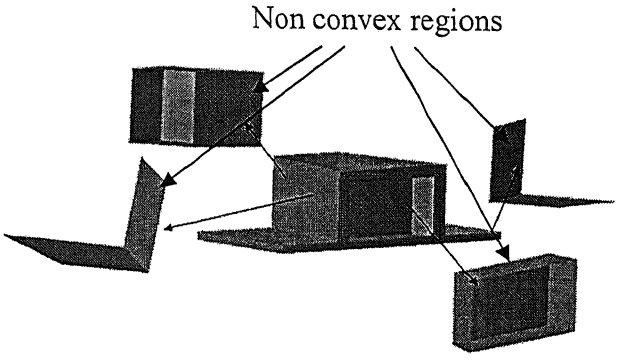

Figure 2.2: A component and its non-convex regions

2.2.1.2 Separation of Interacting Regions

The concept of **mutual concavity** has been developed to identify and separate interacting regions from *isolated non-convex regions* $\{F_i\}$ having no total local visibility zone. The methodology to identify non-convex regions having zero local visibility is described in section 2.2.3.1.

Mutual Concavity: Two facets can be defined as mutually concave if they are facing each other or at least lie on a plane i.e., $\vec{\eta}.\frac{\vec{v}}{|\vec{v}|} \geq 0$ for both the facets as illustrated in fig 2.3.

From all the facets in an *isolated non-convex region* set $\{F_i\}$, a set of facets which are mutually concave to a facet $f_i \in \{F_i\}$, are separated and grouped based on connectivity. Such facet group sets are denoted by $\{MCF_{1i}, MCF_{2i}...MCF_{Ni}\}$. For each group $\{MCF_{ji}\}$ a convexity check is performed to confirm that each facet belonging to $\{MCF_{ji}\}$ is convex $\left(\vec{\eta}.\frac{\vec{v}_{ij}}{|\vec{v}_{ij}|} \leq 0 \text{ for } i=1-3 \text{ and } j=1-3\right)$ to its adjoining facets which are not in $\{MCF_{ji}\}$. If the condition is satisfied the total feature is separated and stored as a subset of the corresponding *isolated non-convex regions* set i.e. $\{MCF_{ji}\} \subset \{F_i\} \subset \{F\}$. The procedure is continued till all the interacting features are separated from each other. An example part and its interacting features are shown in figure 2.5 (a) and (b) respectively. The separation of the interacting features after applying mutual concavity is shown in figure 2.5 (c).

If all the facets constituting an isolated region are mutually concave to each other, then the isolated region can be considered to be a *true-concave* region as shown in figure 2.4. The separated interacting regions hence form *true-concave* regions.

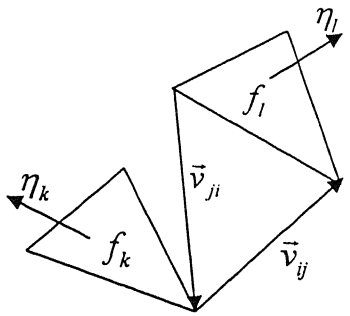

Two facets are said to be *mutually concave* if

i) $\vec{\eta}_k \cdot \frac{\vec{v}_{ij}}{|\vec{v}_{ij}|} > 0$ for i=1 to 3 and j=1 to 3

And

ii) $\vec{\eta}_l \cdot \frac{\vec{v}_{ji}}{|\vec{v}_{ji}|} > 0$ for j=1 to 3 and i=1 to 3

Figure 2.3: A schematic diagram showing mutual concavity between two facets

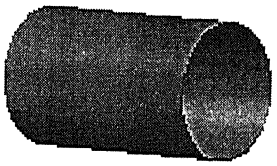

Figure 2.4: An example of true-concave region

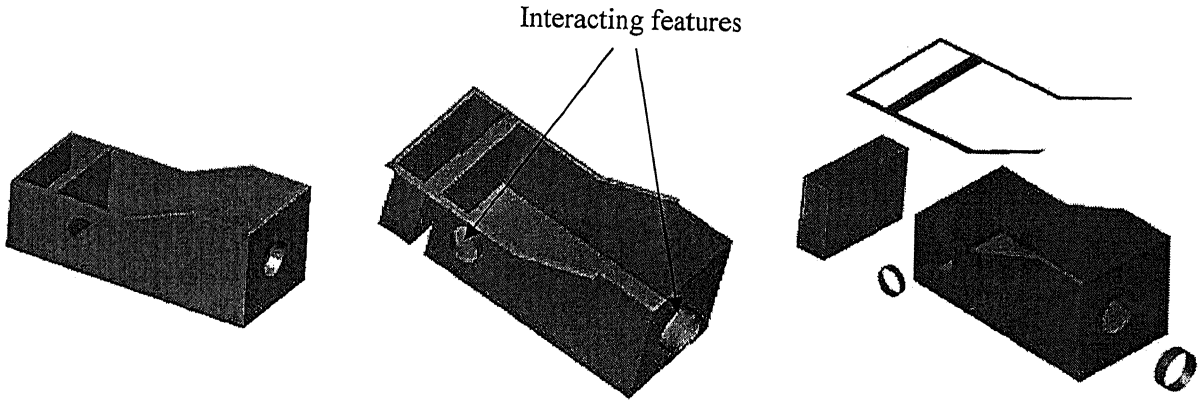

(a) (b) (c)

Figure2.5: (a) An example part with interacting features (b) After non convex regions are identified and grouped. (c) After applying mutual concavity.

Once the non-convex regions and interacting regions are identified and separated, accessibility of the regions along a set of directions is carried out to obtain a pair of direction having minimal obstruction while demoldability. Hence there is the necessity to generate a set of all possible directions along which accessibility testing can be carried out and the same is presented below.

2.2.2 Generation of Probable Visible Directions

The probable list of global viewing directions consists of

(i) Principal axes directions,

(ii) Facet normals,

as used by Priyadarshi et al. [2004]. However there is the requirement to enhance the search space of directions so that a more rigorous visibility checking can be performed. Hence $\vec{d} = \vec{\eta}_i \times \vec{\eta}_j$ with $i \neq j$ is also included in the search space, where $\vec{\eta}_i$, $\vec{\eta}_j$ are the normals of the facets belonging to a particular isolated non convex region. For example for a through cylindrical/conical hole $\vec{d}$ yields its central axis. For freeform surfaces having local depressions, $\vec{d}$ is the direction along which the region can be demolded. In the previous attempts $\vec{d} = \vec{\eta}_i \times \vec{\eta}_j$ was not considered, hence de-molding directions of cylindrical/conical shapes had to be generated by heuristics. While determining the direction set the separated interacting regions are treated as separate non-convex regions. Once the direction set has been generated, the local as well as global accessibility is tested. The procedure used for determining accessibility is presented below.

2.2.3 Accessibility Determination

To define the accessibility of an isolated non-convex region the visibility of the facets constituting the non convex region is tested along specified pair of directions. As proposed by Chen et al. [1993], a non-convex region facet can be blocked only by a non-convex region facet present in the same concave region, i.e. local visibility guarantees global visibility. However this is valid only for non-convex zones having no interacting regions. In the presence of interacting regions $\{MCF_{ji}\}$ in a particular non convex region $\{F_i\}$, the splitting of $\{F_i\}$ into $\{MCF_{ji}\}$ has to be performed. Thus while determining the accessibility of separated interacting regions, the local visibility checking with facets in each $\{MCF_{ji}\}$ and then the global visibility checking with facets in corresponding $\{F_i\}$ is carried out.

2.2.3.1 Local Accessibility and Global Accessibility

The local accessibility checking of a non-convex region is done along facet normals (η_i) and $\vec{d} = \vec{\eta}_i \times \vec{\eta}_j$ of facets constituting the particular region. For a *true-concave* region, if a direction (+***d*** and –***d***) does not provide total visibility, then the direction is not a valid one. Further, if no local directions provide complete visibility of a true concave region, the region can be demolded only by the use of split cores. The present system is not capable of handling products requiring split cores, but it can identify such regions.

All the valid local directions are considered and a direction set is created. The global accessibility/visibility of each non-convex region is tested along each direction (+***d*** and –***d***). Accessibility test of a facet f_i with respect to another facet f_j along a direction involves two major steps and they are:

(i) Determination of the location of facet f_i with respect to facet f_j

(ii) Determination of obstruction of facet f_i with respect to facet f_j by projecting the facets on a plane perpendicular to the viewing direction.

The two steps are presented below in detail.

2.2.3.2 Facet Location

The normals of the facets bounding the object always point away from the inside region. Any direction vector ***d*** lying in the unit hemisphere with the facet normal as the pole can be defined to be a probable visible direction for that facet as shown in figure 2.6 and the facet is front facing with respect to it as shown in the figure 2.7. Otherwise it is back facing and invisible along $+\boldsymbol{d}$ but probably visible along $-\boldsymbol{d}$. Hence for a facet having a normal η and a pair of directions $+\boldsymbol{d}$ and $-\boldsymbol{d}$ the probable visible directions can be summarized as:

(i) If $\boldsymbol{d}.\eta > \tau$, the facet is probably visible in $+\boldsymbol{d}$ direction,

(ii) Else if $\boldsymbol{d}.\eta < \tau$, the facet is probably visible in $-\boldsymbol{d}$ direction,

(iii) Else the facet is probably visible along both $+\boldsymbol{d}$ and $-\boldsymbol{d}$ directions.

A facet can be considered to be vertical/perpendicular (defined by its normal) with respect to a direction if its normal η makes an angle of $88^\circ - 92^\circ$ with that direction as shown in figure 2.8. The τ value acts as a bounding value based on which the facets can be classified as vertical and non-vertical facet. Hence the value of τ ranges between -0.035 to 0.035 ($\cos(88^\circ) = 0.035$ to $\cos(92^\circ) = -0.035$) to determine the visible direction of the facets.

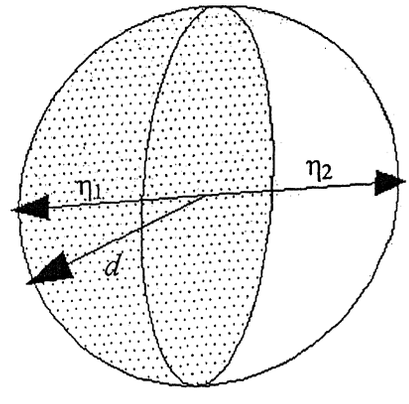

Figure 2.6: Figure showing the probable visibility zone of a facet having normal η_1

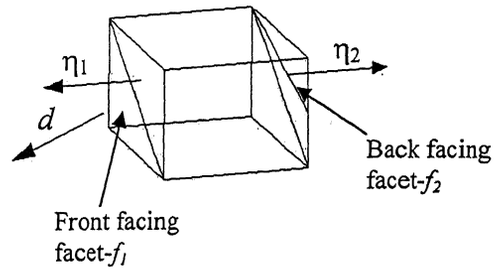

Figure 2.7: An example showing front facing and back facing facets

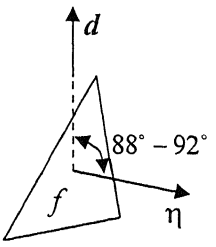

Figure 2.8: Criteria to classify a facet as perpendicular facet is shown

Once it is decided that a facet is probably visible along $+\boldsymbol{d}$ or $-\boldsymbol{d}$ or both the directions, an intersection check is performed to guarantee its visibility along the pair of directions. To check the visibility along any pair of directions ($+\boldsymbol{d}$ and $-\boldsymbol{d}$), the $+\boldsymbol{d}$ direction is made the +z-axis of the new coordinate system and corresponding transformation of facet vertices and normals is made (see Appendix A). Thus the visibility checking of a front facing facet is performed with only the facets lying above it because it is already obscured in $-\boldsymbol{d}$ direction and vice versa. However for facets probably visible in both directions (perpendicular facets) visibility check is performed with all facets lying above or below it.

The relative position of a facet (f^1) with respect to another facet (f^2) is decided as follows:

If $z^1_i < z^2_j$ for i=1 to 3 and j=1 to 3, then f^1 lies absolutely below f^2,

Else if $z^1_i > z^2_j$ for i=1 to 3 and j=1 to 3, then f^1 lies absolutely above f^2.

The two facets lie on the same plane if $z^1_i \approx z^2_j$. The z^1_i, z^2_j are the transformed z-coordinates of the facet vertices. However cases may arise where the facets may not be located absolutely above or below each other as shown in figure 2.9 (a) and 2.9 (b) respectively. In such a situation the vertices of facet f_1 are projected along the direction of viewing $\boldsymbol{d}$ on the plane defined by facet f_2. The point of intersection is obtained by considering intersection of a line with a plane (see Appendix B). The equation of the line is obtained by joining (x_i, y_i, z_i) with (x_i, y_i, z_2) where z_2 is z-coordinate of any vertex of f_2 as shown in figure 2.10. If for all vertices of f_1, $z_{\text{intersect}} < z_{\text{facet}}$ then f_1 lies above f_2 as shown in figure 2.9 (b). Else for all vertices of f_1, if $z_{\text{intersect}} > z_{\text{facet}}$ then f_1 lies below f_2 as shown in figure 2.9 (a). Otherwise two cases may arise: (i) both the facets may lie on the same plane and there cannot be any intersection between them, or (ii) the facets have a critical orientation as shown in figure 2.11. Situation (ii) can be resolved by transforming f_1 and f_2 along normal of f_1 as +z direction and checking whether $z_{f1} <$ or $> z_{f2}$ where z_{f1} and z_{f2} are the transformed z-coordinates of the facets vertices of facets f_1 and f_2 respectively. Once the relative location of two facets is decided, obstruction checking is performed to ensure whether f_1 is visible along the viewing direction.

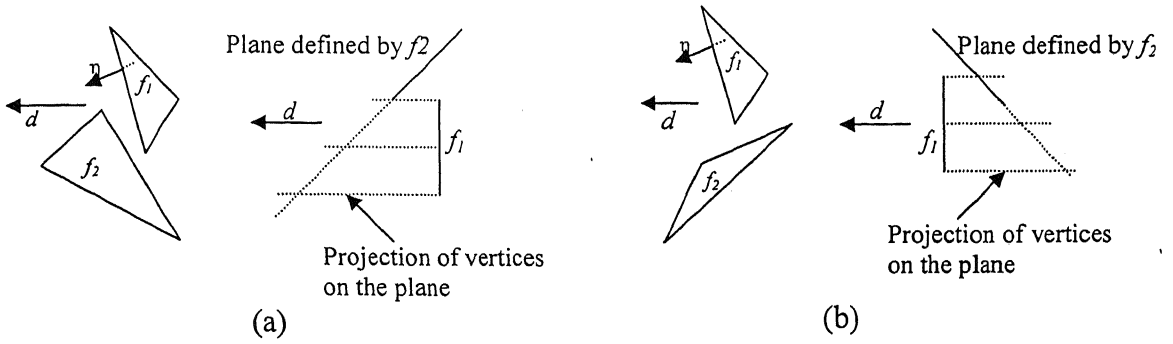

Figure 2.9: (a) Schematic diagram showing f_2 lying above f_1.
(b) Schematic diagram showing $f2$ lying below f_1.

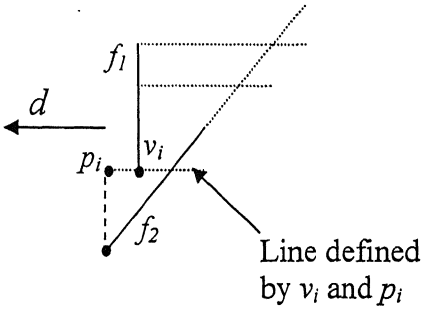

Figure 2.10: Schematic diagram showing the projection of facet f_1 on facet f_2 along $\boldsymbol{d}$

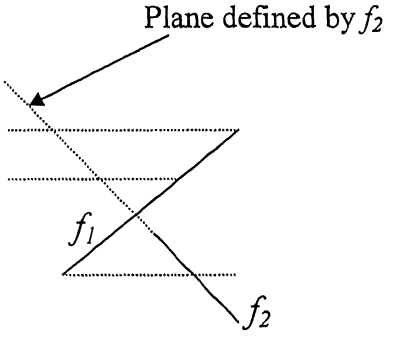

Figure 2.11: Schematic diagram showing the critical orientation between two facets when all $z_{intersect} <$ or $> z_{original}$ fails.

2.2.3.3 Facet Obstruction Determination

The facet intersection is tested by projecting the two facets on the plane perpendicular to $+d$ or $-d$ and their intersection is tested by *separating axis condition* [see Appendix C]. Visibility is guaranteed if there is no obstruction between the two facets. A facet is said to inaccessible if it is totally or partially obstructed.

A *true-concave* region must have total visibility along a pair of direction. Else it is invisible along the particular pair of direction. *Non-true-concave* regions may or may not be totally visible along a pair of directions. For example, for the *non-true-concave* region shown in figure 2.12 (b) of the example part shown in figure 2.12 (a), complete visibility does not exist along any particular pair of direction but over a set of directions as shown in figure 2.12 (c). For such regions initially a list of local directions and corresponding visible facets is made. Then it is checked that the region is totally visible along the set of directions. If it is not then the region can only be molded by means of split core. A list of directions with corresponding visible *true-concave* regions and facets of partially visible *non-true-concave* regions is made. The total visible surface area of *non-true-concave* regions and the number of visible *true-concave* regions along each pair of directions is also stored.

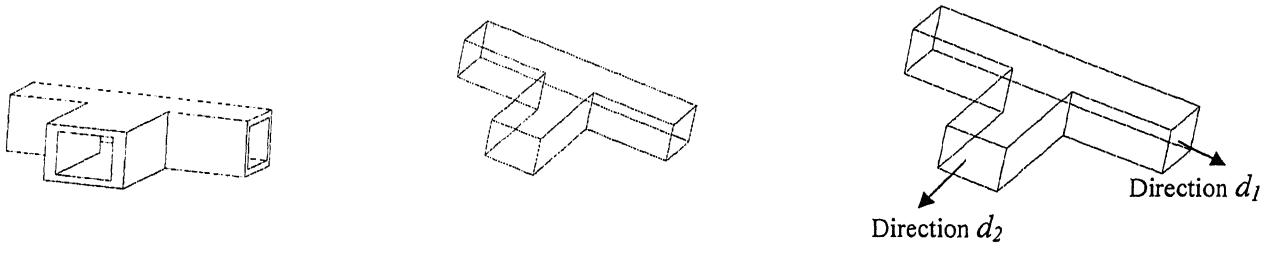

Figure 2.12: (a) An example part. (b) Non *true- concave* non- convex region not visible completely along any direction pair $+\boldsymbol{d}$ and $-\boldsymbol{d}$. (c) The region completely visible along direction set $\boldsymbol{d_1}$ and $\boldsymbol{d_2}$.

2.3 Flatness of Parting Line

From the literature review [section 1.2.2] it can be inferred that flatness of parting line influences the cycle time and manufacturing complexity of the product. The flatness of parting line achievable along each pair of direction is defined by *flatness factor* (FF) and can be represented by equation 2.1.

$$\text{Flatness factor } FF(d) = \sum_{i=1}^{k} length(\hat{e}_i) / \sum_{i=1}^{k} length(e_i) \qquad (2.1)$$

where e_i's are the line segments constituting the parting line and $\hat{e}_i$'s their projections on a plane perpendicular to d [Majhi et al., 1999]. Hence $0 < FF(d) \leq 1$ and in the best case i.e. parting line lying on a plane, $FF(d) = 1$.

To obtain the parting line segments along a pair of direction the facets are separated as positive facets (visible along $+\boldsymbol{d}$), negative facets (visible along $-\boldsymbol{d}$) and perpendicular facets (visible along both directions). Three cases may arise:

(i){Perpendicular facets} = NULL. In such cases the common edges of the facets belonging to {Positive facets} and {Negative facets} define the parting line.

(ii) There are no common edges between {Positive facets} and {Negative facets}. The parting line in this case will pass through the {Perpendicular facets}.

(iii) There are common edges between {Positive facets} and {Negative facets} but they don't form a close loop.

The detailed methodology to obtain the most optimal parting line is discussed in section 3.2. Once the parting line segments are determined, the flatness factor is obtained by using equation 2.1. The projected length of the parting line $\sum_{i=1}^{k} length(\hat{e}_i)$ is determined by transforming the edge vertices considering direction $+d$ as +z direction of the new coordinate system and length of each line segment is obtained by $\sqrt{(x_1 - x_2)^2 + (y_1 - y_2)^2}$. Similarly true length of the parting line $\sum_{i=1}^{k} length(e_i)$ can be determined by $\sqrt{(x_1 - x_2)^2 + (y_1 - y_2)^2 + (z_1 - z_2)^2}$.

2.4 Determination of Draw Depth

The draw depth (DD) along a particular direction is obtained by transforming the vertices of the part by considering direction $+d$ as the +z axis of the transformed coordinate system. The difference of the maximum and minimum z-dimensions produces the draw depth as shown in equation 2.2.

$$DD = z_{max} - z_{min} \qquad (2.2)$$

2.5 Selection of Parting Direction

Factors related to the extent of visibility, flatness of parting line and relative draw depths are evaluated for all possible parting directions. The determination of *flatness factor* is already discussed in section 2.2. Two other factors (i) *visibility factors* (ii) *draw depth factor* for each parting direction pair is evaluated and is presented below.

Visibility Factors ($VF_1(d)$ and $VF_2(d)$):

Visibility Factors give the extent of visibility along a given parting direction. When *true concave* regions are present the number of visible *true-concave* regions is considered to obtain visibility factor. It can be expressed as given below.

$$VF_1(d_i) = \frac{Number\ of\ visible\ true\ concave\ regions}{Total\ Number\ of\ true\ concave\ regions}$$

For *non-true-concave* regions the surface area of *non-true-concave* regions is considered. It can be expressed as given below.

$$VF_2(d_i) = \frac{Surface\ area\ of\ visible\ non\ convex\ facets}{Surface\ area\ of\ non convex\ facets}$$

Thus $0 \le VF_1(d_i) \le 1$ and $0 \le VF_2(d_i) \le 1$. In the best case, i.e. when there are no undercuts, $VF_1(d_i)$=1 and $VF_2(d_i)$=1.

Draw Depth Factor (*DDF (d)*):

Draw depth factor (*DDF (d)*) is defined as given below.

$$(DDF(d_i) = 1 - \frac{DD(d_i)}{DD_{\max}(d)}$$

where *DD* (d_i) is the draw depth along a given pair of direction and $DD_{\max}(d)$ is the maximum of all the draw depths amongst all the candidate parting directions. Thus $0 \le DDF(d_i) < 1$ and in the worst case, i.e. direction having maximum draw depth, $DDF(d_i) = 0$.

Overall factor (*OF* (d_i)):

An Overall factor *OF* (d_i) which gives a measure of the cumulative influence of all the four factors for all the candidate parting directions is obtained and can be represented as shown below:

$$OF(d_i) = VF_1(d_i) + VF_2(d_i) + FF(d_i) + DDF(d_i)$$

To determine an optimal parting direction weighted contribution of all the factors can be considered while determining the overall factor *OF* (d_i) and the modified expression is shown below:

$$OF(d_i) = \frac{w_1 VF_1(d_i) + w_2 VF_2(d_i) + w_3 FF(d_i) + w_4 DDF(d_i)}{\sum_{i=1}^{4} w_i}$$

w_i's are the weightages assigned to each factor.

The optimal parting direction will be the one which will have highest value of $OF(d_i)$.

2.6 Selection of Side Core/Cavity Direction

The side core/cavity directions for a given parting direction are selected from the list of directions along which accessibility of non convex regions has been checked. A search is made in the direction list to obtain those directions $\{d_u\}$ along which atleast one of the undercuts (for the given parting direction) is visible. Surface area of visible undercut regions SA_u is calculated for each direction in $\{d_u\}$. From $\{d_u\}$ the direction that maximizes SA_u is chosen as the side core/cavity direction. If all the non convex regions are still not moldable by the combination of main parting direction and side core/cavity direction, a similar search is carried out in the direction list to obtain the side core/cavity direction for the remaining undercuts. The procedure is continued till all the non-convex regions are moldable by the combination of main parting direction and side core/cavity directions.

Chapter III

Determination of Parting Line and Parting Surface

3.1 Introduction

The location and flatness of parting surface has a substantial influence on the productivity and quality of the final product. A flat parting surface is the most desired one since it reduces the time and cost involvement in manufacturing of the dies and molds and also makes the design of the clamping system easier (section 1.2.2). Parting line gives a direct measure of the parting surface.

In the present work, an attempt is made to determine and generate the flattest parting line for a given parting direction. An attempt to generate the flattest parting line for a given parting direction has been made by Majhi et al. [1999] but it is applicable only to convex polyhedral objects. The presence of undercuts is also not considered in their attempt. The present work takes into consideration the location of undercuts and is applicable to any form of solid object. The procedure to identify the true-non-convex perpendicular regions is described in section 3.2.1. The methodology to generate the parting line taking into consideration the location of undercuts and constraining non-convex non-perpendicular regions is described in sections 3.2.2 and 3.2.3. Once the parting line is determined, parting surface generation is done using the methodology developed by Fu et al. [2001] and is described in section 3.3.

3.2 Determination and Generation of Parting line

As discussed in the previous chapter the visible facets can be grouped as positive facets (visible in $+\boldsymbol{d}$ direction), negative facets (visible in $-\boldsymbol{d}$ direction) and perpendicular facets (visible in both directions) in order to determine the parting line. The $+\boldsymbol{d}$ direction is made the $+z$ axis of the new coordinate system and transformations are made accordingly (see Appendix A) prior to generating the parting line. If there are no perpendicular facets then the parting line is usually the collection of the common edges of positive and negative facets. However situations may arise where there may be a closed region of perpendicular facets between positive and negative facets (Fig 3.1) or there may be common edges of positive and negative facets separated by perpendicular facet groups (Fig 3.2). Majhi et al. [1999] developed an algorithm for above mentioned cases but it is valid only for convex polyhedral objects. However non-convex facets may be present in the set of perpendicular facets. Prior to generation of parting line, there is a need to identify those non-convex perpendicular facets that form the bounding surface of the object. In the present work, an attempt has

been made to generate flattest parting line for a typical 3-D component having convex as well as non-convex regions along a given parting direction.

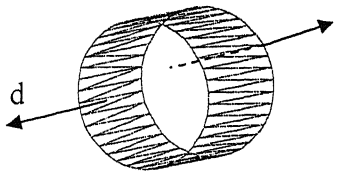

Figure 3.1: A schematic diagram showing close loop of perpendicular facets

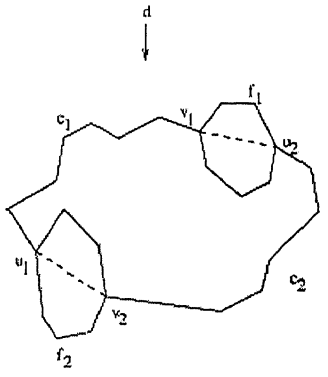

Figure 3.2: A schematic diagram showing common edges of positive and negative facets separated by perpendicular facet groups

3.2.1 Identification of True Non-convex Perpendicular regions

To identify the true non-convex perpendicular regions, a connectivity test is performed between the non-convex perpendicular facet groups $\{F^{ncp}\}$ with the common edges of positive and negative facets $\{e^{pn}\}$ (if present) and the convex perpendicular facets $\{f^{cp}\}$. If any facet in a facet group $\{F_i^{ncp}\}$ has any common vertex with the common edges of positive and negative facets $\{e^{pn}\}$ (if present) or the convex perpendicular facets $\{f^{cp}\}$ then the facet group $\{F_i^{ncp}\}$ forms a true non-convex perpendicular region. An example of true non-convex perpendicular region is shown in figure 3.3 (b). For the same part [Fig 3.3 (a)] but for a different parting direction a facet region not forming a true non-convex perpendicular region is shown in figure 3.3 (c).

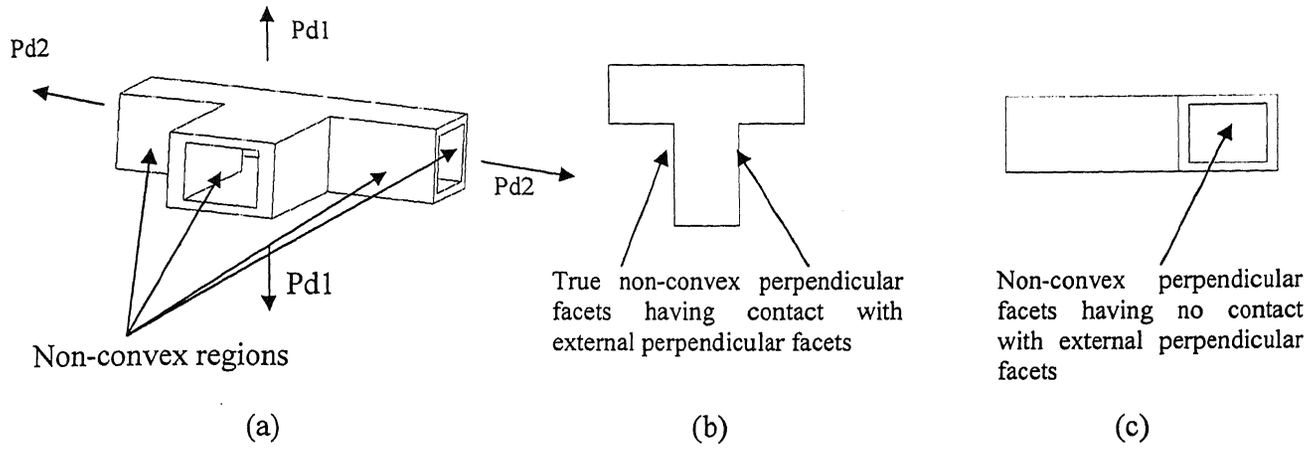

Figure 3.3: (a) An example part. (b) True non-convex perpendicular facets along Parting direction1. (c) Non-true non-convex perpendicular facets along Parting direction2.

3.2.2 Close loop of Perpendicular Facets

When there are no common edges between the positive and negative facet groups and perpendicular facet set is not NULL, the parting line may pass through the perpendicular facet set. The perpendicular facet set is projected on the plane perpendicular to ***d*** and the existence of closed loop is tested to guarantee whether the parting line can be located on the perpendicular facet set or not. Once it is guaranteed that the parting line can be located on the perpendicular facet set, the z_{min} of the positive region and z_{max} of negative region is obtained. Only those non-convex non-perpendicular regions that remain in contact with convex perpendicular facets can affect the parting line location and hence they are considered. Those that do not remain in contact forms the projections and/or depressions on the molds and do not impose any constraint on the location of parting line. The procedure to obtain such regions is described below.

The boundary edges of the non-convex non-perpendicular facet groups $\{F_i^{ncnp}\}$ are identified and they are projected on the x-y plane of the new coordinate system to obtain the edge groups $\{be_i^{ncnp}\}$. The convex perpendicular facets $\{f^{cp}\}$ are also projected on the x-y plane of the new coordinate system to obtain the edge groups $\{e^{cp}\}$. A connectivity test of each edge group $\{be_i^{ncnp}\}$ is performed with the edge groups $\{e^{cp}\}$ to ensure whether the edge group $\{be_i^{ncnp}\}$ is the constraining region or not. If any of the ends of an edge e_i of edge group $\{be_i^{ncnp}\}$ lies within or on the edge e_j of edge groups $\{e^{cp}\}$ then the corresponding non-convex non-perpendicular region is connected and is a constraining region. To check whether an end of an edge e_i lie inside or on other edges e_j the distance $d_i = \sqrt{(x_i - x_j)^2 + (y_i - y_j)^2}$ (where i=the particular end of edge e_i and j=1,2

the ends of another edge e_j) is calculated. The distance d_j between the ends of edge e_j is also calculated. If $\sum_{i=1}^{2} d_i = d_j$ then it can be concluded that edge e_i lies within or on edge e_j. An example showing a constraining region and a non-constraining region is shown in figure 3.4 (a) and 3.4 (b) respectively.

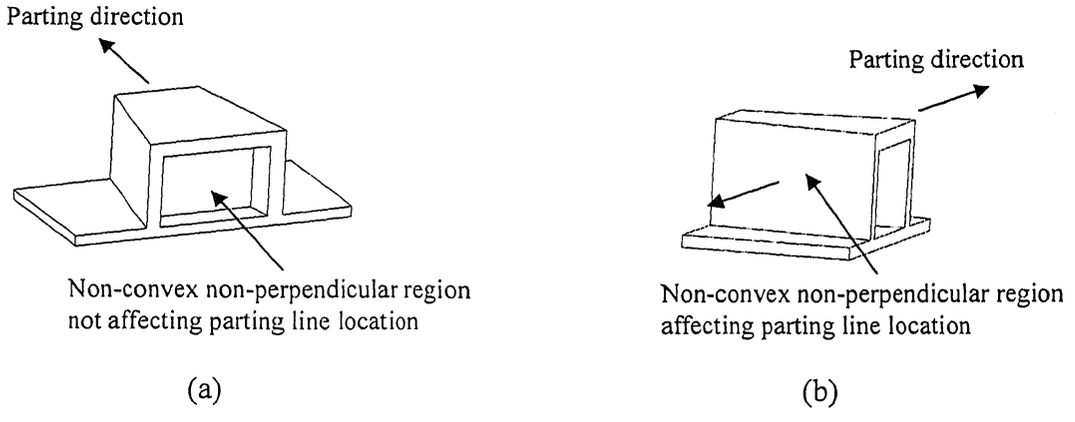

Figure 3.4: An example part showing (a) Non-constraining non-convex non-perpendicular region. (b) Constraining non-convex non-perpendicular region

Before generating the parting line passing over close loop of perpendicular facets, a parting plane which contains the parting line is defined. In the absence of undercuts, a plane perpendicular to ***d*** (+z direction of the transformed coordinate system) and passing through $z_{location}$ (equation 3.1) is the desired plane. Such a parting line location reduces the draw depth. However, in the presence of undercuts the parting plane is preferably located at $z_{location} = z_{min}$ of the positive region or $z_{location} = z_{max}$ of negative region, since in processes such as injection molding or die casting, side core/cavities are usually preferred on any one of the mold halves (preferably the core). The parting line must not intersect the undercuts since it increases the tolerance required. Hence, in order to avoid intersection the extreme position of the undercuts ($z_{min}^{undercut}$ and $z_{max}^{undercut}$) are calculated and it is checked that z_{min} of the positive region > $z_{max}^{undercut}$ or z_{max} of negative region < $z_{min}^{undercut}$. If this condition is satisfied the parting line is generated using the methodology described in section 3.2.2.1. Else, the parting line is generated using the methodology described in section 3.2.2.2 In the absence of undercuts, if z_{max} of negative region > z_{min} of the positive region, a flat parting line passing over the perpendicular facets is not possible. The best parting line for such cases is constructed as described in section 3.2.2.2.

$$z_{location} = \frac{z_{positive}^{min} + z_{negative}^{max}}{2} \qquad (3.1)$$

3.2.2.1 Flat Parting Line passing over Perpendicular Facets possible

The parting line is generated by intersecting the perpendicular facets by a plane perpendicular to ***d*** (+z direction of the transformed coordinate system) and passing through pt = (0, 0, $z_{location}$) where $z_{location}$ is obtained from equation 3.1 or it is z_{min} of the positive region or z_{max} of negative region . The bounding edges of each facet are intersected by the plane and the intersecting points are joined to generate the parting line edges. An edge of a facet is intersected by the plane if $v_1 \geq z_{location}$ and $v_2 \leq z_{location}$ or vice versa, where v_1 and v_2 are the edge vertices. The intersecting point is obtained by considering intersection of line with a plane (see Appendix-B).

3.2.2.2 Flat Parting Line passing over Perpendicular Facets not possible

The perpendicular facet groups are attached with the positive or negative facets in as many combinations as possible. If there are n number of perpendicular facet groups then the number of possible arrangements are $\frac{n}{2}(n+1)+1$. For each arrangement there will be a different set of perpendicular positive facets and perpendicular negative facets. For each arrangement the common edges between the positive facets and perpendicular negative facets, the negative facets and perpendicular positive facets, and perpendicular positive facets and perpendicular negative facets is obtained. It is checked whether the common edges form a close loop or not. If the edges form a close loop then the *Projected Perimeter* and the *Flatness Factor* (equation 2.1) is calculated. The *Projected Perimeter* d_p is obtained by summing the projected edge lengths as shown in equation 3.2.

$$d_p = \sum_{k=1}^{N} \sqrt{(x_{1k} - x_{2k})^2 + (y_{1k} - y_{2k})^2} \qquad (3.2)$$

where N is the number of edges.

The arrangement giving the maximum flatness factor value is chosen as the best arrangement. If however the *Flatness Factor* of two arrangements is equal then the arrangement having a greater *Projected Perimeter* is selected as the best arrangement and the corresponding parting line is the best parting line.

3.2.3 Disjointed Common Edges

A condition may arise when there are disjointed sets of common edges of positive and negative facets separated by valid perpendicular set of facets (Fig. 3.2). If the projection of these facets on a plane perpendicular to ***d*** yields a close loop, then a parting line passing through the perpendicular facets and common edges is possible. Three categories of perpendicular facet regions are obtained as shown in figure 3.5 and they are as follows:

(i) Region bounded on both sides by common edge end points.

(ii) Region bounded on one side by common edge end point and free on the other.

(iii) Unbounded regions.

The methodologies to obtain the best parting line for such cases are discussed in sections 3.2.3.1, 3.2.3.2 and 3.2.3.3 respectively.

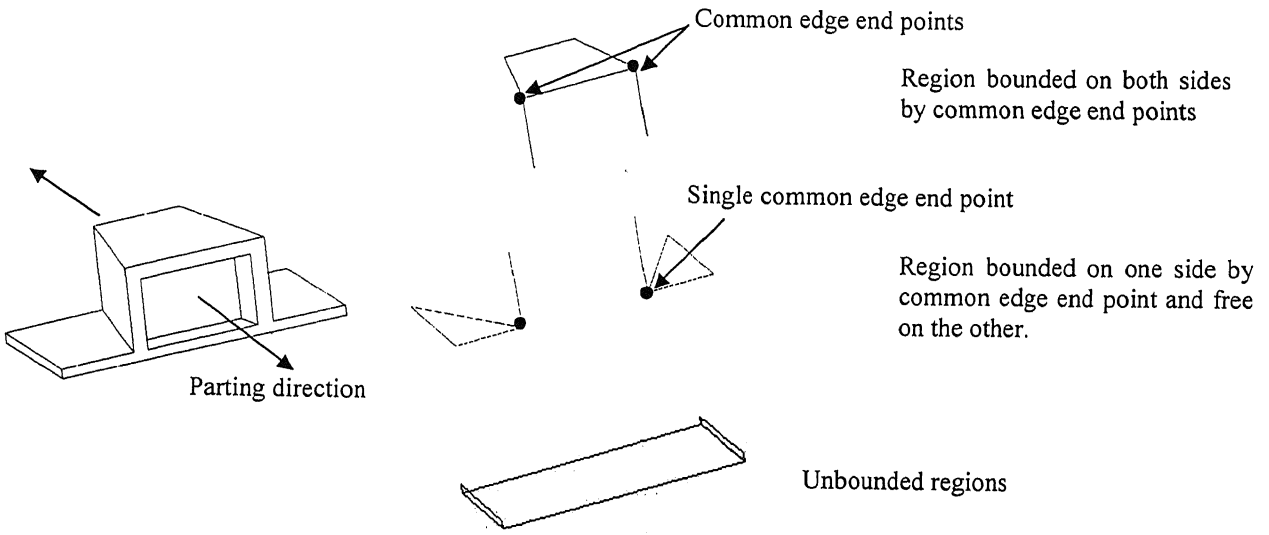

Figure 3.5: Example of different categories of perpendicular facet region for the parting direction shown.

3.2.3.1 Region bounded on both sides by Common Edge end points

The parting line should pass through the plane defined by the following:

(i) It must contain the vector $\vec{v} = \vec{E}_2 - \vec{E}_1$ where $\vec{E}_2$ and $\vec{E}_1$ are the common edge ends as shown in figure 3.6.

(ii) It must be perpendicular to the plane containing $\vec{v}$ and $\vec{d}$ (the $+z$ direction of the new coordinate system).

(iii) It must pass through one of the common edge ends $\vec{E}_1$ or $\vec{E}_2$.

The desired plane is shown in figure 3.6. The normal $\vec{\eta}_{plane}$ of the plane can be obtained to be $\vec{\eta}_{plane} = \vec{d} - \left(\vec{d}.\frac{\vec{v}}{|\vec{v}|}\right)\frac{\vec{v}}{|\vec{v}|}$ as shown in figure 3.7. Once the plane containing the parting line is defined the parting line segments are generated as discussed in section 3.2.3.1.1.

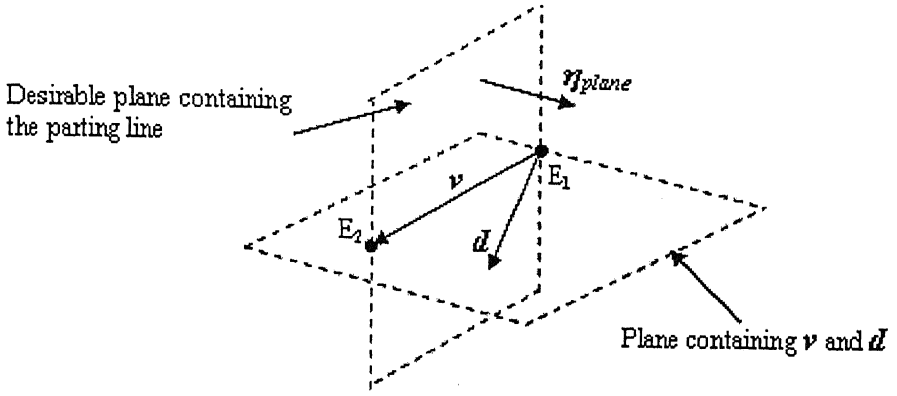

Figure 3.6: The desirable plane for region bounded on both sides by common edge end points.

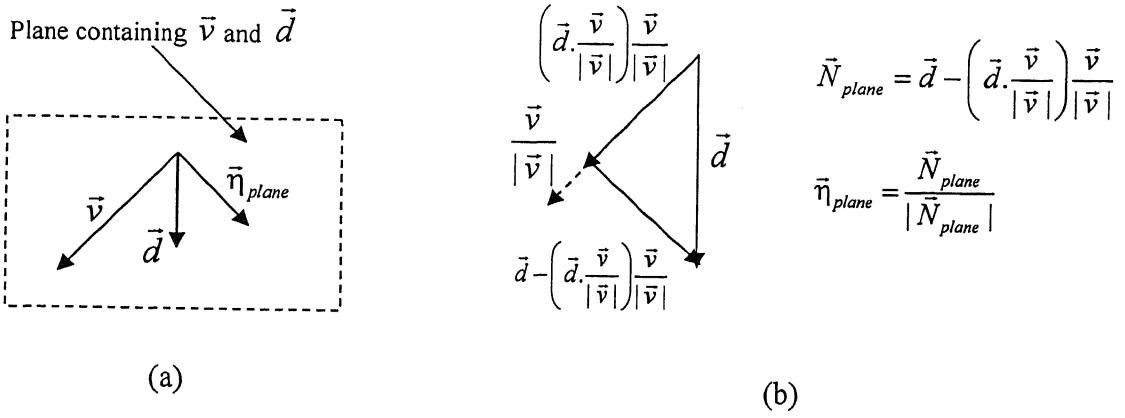

Figure 3.7: Schematic diagram showing (a) Normal $\vec{\eta}_{plane}$ of the plane containing the parting line. (b) Derivation of the normal $\vec{\eta}_{plane}$.

3.2.3.1.1 Procedure to generate the Parting Line

Once the parting plane is defined, the procedure to generate the parting line segment is initiated by considering $\vec{E}_1$ as the first point pt i.e $pt = \vec{E}_1$. A set of facets f_k adjacent to pt is considered. A facet is said to adjacent to pt if the condition stated below is satisfied.

$$length(pt - p^i_{f_k}) + length(pt - p^j_{f_k}) = length(p^i_{f_k} - p^j_{f_k}) \text{ and } i \neq j$$

where $p^i_{f_k}$, $p^j_{f_k}$ are the vertices of the k_{th} facet. A flat parting line is possible if the plane passing through $\vec{E}_1$ and having normal $\vec{\eta}_{plane}$ intersect the edges of the adjacent facets on the plane itself. The intersection point $\vec{p}_{ij}$ can be obtained by using the equations from 3.3 to 3.5:

$$(\vec{p}_{ij} - \vec{E}_1).\vec{\eta}_{plane} = 0 \qquad (3.3)$$

$$\vec{p}_{ij} = \vec{p}^{\,i}_{f_k} + u(\vec{p}^{\,j}_{f_k} - \vec{p}^{\,i}_{f_k}) \tag{3.4}$$

$$u = \frac{(\vec{E}_1 - \vec{p}^{\,i}_{f_k}).\vec{\eta}_{plane}}{(\vec{p}^{\,j}_{f_k} - \vec{p}^{\,i}_{f_k}).\vec{\eta}_{plane}} \tag{3.5}$$

If $0 \le u \le 1$, $\vec{p}_{ij} \neq \overrightarrow{pt}$ and absolute value of $(\vec{p}^{\,j}_{f_k} - \vec{p}^{\,i}_{f_k}).\vec{\eta}_{plane} > 0$ is satisfied then $\vec{p}_{ij}$ is on the plane defined by $\vec{\eta}_{plane}$. If $\vec{p}_{ij}$ satisfies equation (3.3) it means that $\vec{p}_{ij}$ lies on the parting plane defined by $\vec{\eta}_{plane}$. The parting plane actually intersects the line segment formed by $\vec{p}^{\,j}_{f_k}$ and $\vec{p}^{\,i}_{f_k}$ if $0 \le u \le 1$. Such a point is shown in figure 3.8. However if this fails a vertex which is least deviated from the plane perpendicular to $\vec{\eta}_{plane}$ (equation 3.6) and belonging to the set of adjacent facets f_k of point *pt* is considered as shown in figure 3.9.

$$\vec{p}_{ij} = \min\left(abs\left(\vec{\eta}_{plane} \cdot \frac{(\vec{p}_{ij} - \vec{E}_1)}{|(\vec{p}_{ij} - \vec{E}_1)|} \right) \right) \tag{3.6}$$

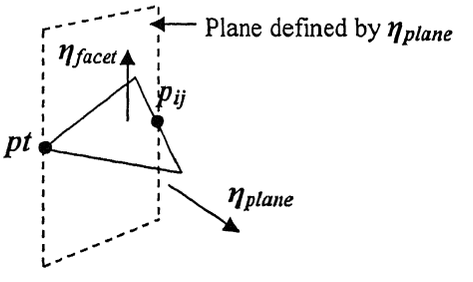

Figure 3.8: Intersection of the plane with the edge of an adjacent facet.

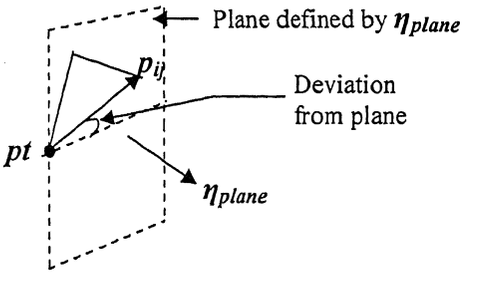

Figure 3.9: The deviation of the vector from the plane containing the parting line.

It may be possible that the intersecting point $\vec{p}_{ij}$ actually reverses the direction of parting line development. Hence from the set of all intersecting points or least deviated points the one that satisfies equation 3.7 is selected.

$$\vec{p}_{intersect} = \max\left(\left(\frac{(\vec{p}^{\,i}_{intersect} - pt)}{|\vec{p}^{\,i}_{intersect} - pt|}\right).\left(\frac{(pt - pt_{previous})}{|pt - pt_{previous}|}\right)\right) \quad (3.7)$$

where i=1 to n are the number of intersecting points and $pt_{previous}$ is the point previous to pt.

The procedure is continued till next edge $\vec{E}_2$ is reached.

3.2.3.2 Region bounded on One side by Common Edge end point and free on the other

Only a single common edge end is available in this case. Hence before moving on with the procedure to obtain the parting line the other extreme point has to be defined. This is done by projecting the perpendicular facets belonging to the particular set on the plane perpendicular to $\vec{d}$ (+z direction of the transformed coordinate system). To obtain the edge formed due to the projection of a facet f on the x-y plane, (x_i, y_i) coordinates of its vertices are considered. The projection of a perpendicular facet on the x-y plane generates a line containing the three vertices as shown in fig 3.10 (a). The distance between the vertices ($d_k = \sqrt{(x_i - x_j)^2 + (y_i - y_j)^2}$ where $i \neq j$) is calculated. The vertex pair giving the maximum distance is considered as the edge ends and the third vertex is excluded as shown in fig 3.10 (b). Only a chain of edges connected at edge ends is constructed. Hence if any edge (e_i) has one or both of its ends lying inside another edge (e_j) in the same edge group then the edge ends are modified and is described below.

To check whether an edge end of an edge e_i lie inside other edges e_j, the distance ($d_i = \sqrt{(x_i - x_j)^2 + (y_i - y_j)^2}$ where i=the particular end of edge e_i and j=1,2 are the ends of another edge e_j) is calculated. The distance d_j between the ends of edge e_j is also calculated. If $\sum_{i=1}^{2} d_i = d_j$ and $d_i \neq 0$ then the particular end of edge e_i lie inside edge e_j. If both the ends of edge e_i lie inside edge e_j then edge e_i is excluded from the chain of edges (Fig.3.11). If one of the edge ends of edge e_i lies inside edge e_j then the two vertices lying farthest apart are joined to generate a new edge (Fig.3.11) since for projected perpendicular facets such a condition implies that the edges are collinear.

From the set of projected edges the edge ends having no connectivity is considered. One of the edge ends will be the common edge end point $\vec{E}_1$. The x and y values of the other edge end (E_2^x and E_2^y) gives the other extreme point. A plane perpendicular to $\vec{d}$ (+z direction of the transformed coordinate system) and passing through one of the common edge point $\vec{E}_1$ is considered. The

procedure as described in section 3.2.3.1.1 is then exactly followed till $pt_x = E_2^x$ and $pt_y = E_2^y$ is satisfied.

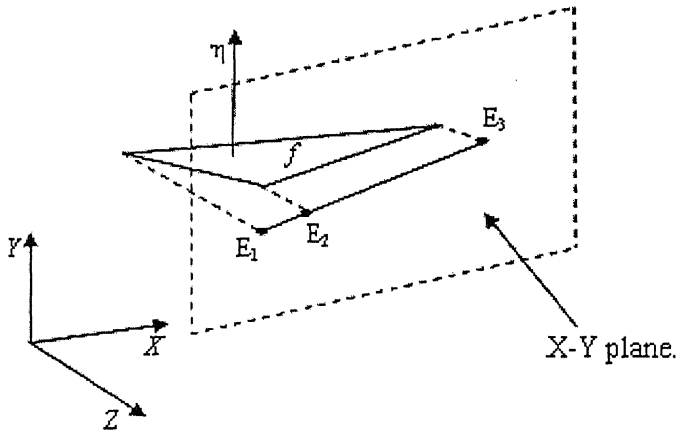

(a)

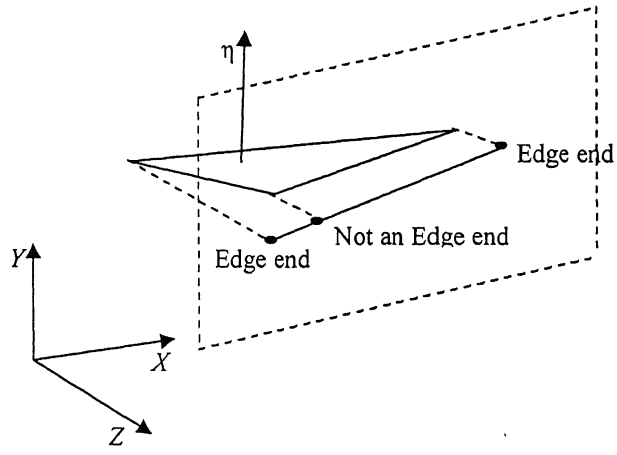

(b)

Figure 3.10: Schematic diagram showing (a) Projection of perpendicular facet on x-y plane. (b) Generation of edge ends

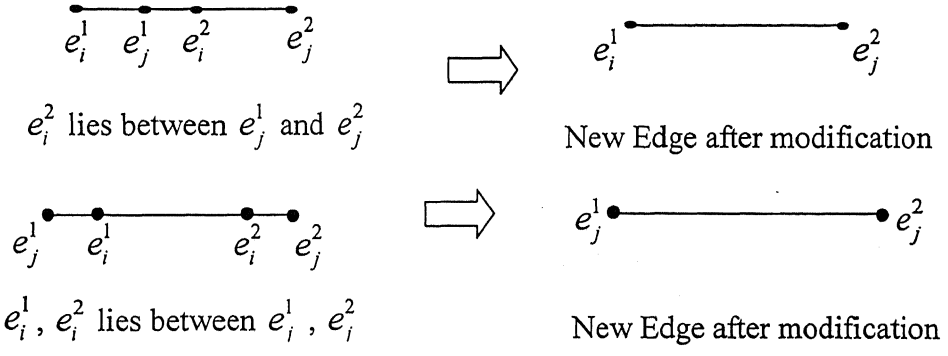

Figure 3.11: Diagram showing modification of edges.

3.2.3.3 Unbounded Regions

Once parting line segments for regions bounded on one side by common edge end point and free on the other is obtained, the unbounded regions get bounded. The procedure for regions bounded on both sides by common edge end points (section 3.2.3.1) is then followed to obtain parting line segments for such cases.

3.3 Generation of Parting Surface

Once the 3-D parting line is determined the parting surface is obtained by using the methodology of extrusion developed by Fu et al. [2001]. The methodology has certain limitations. Firstly, it cannot handle cases when the extrusion of the edge along a direction is obstructed. An example of such a case is shown in figure 3.12. An attempt has been made by C L Li [2002] where parting surfaces for such cases have been generated by using Catmull Clark subdivision method. Secondly, the parting surface generated will have a rectangular boundary parallel to x and y axes. This may give unsatisfactory results in certain cases as shown in the figure 3.13.

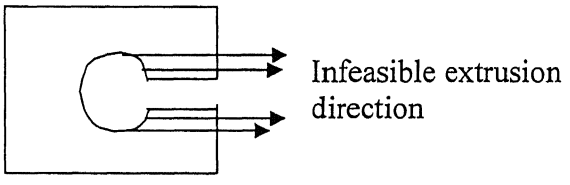

Figure 3.12: Parting line having obstruction while extrusion.

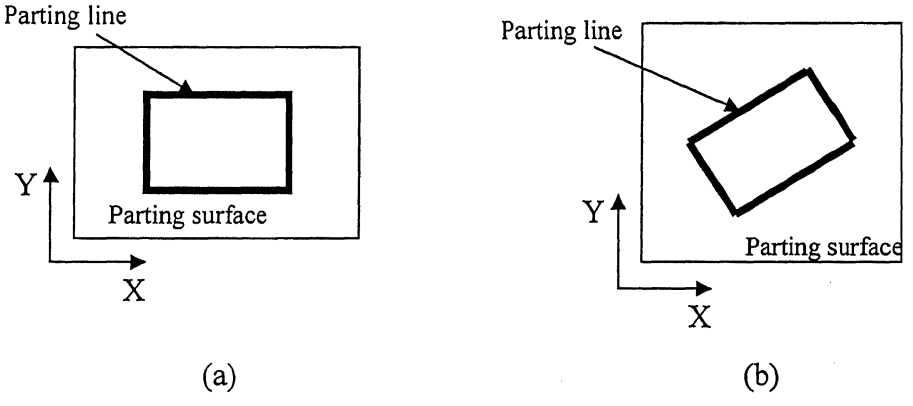

Figure 3.13: (a) Desirable Parting line orientation.
(b) Undesirable Parting line orientation

Before extruding the parting line segments it is essential to identify the direction of extrusion of the line segments. For this purpose the parting line segments are projected on the X-Y plane perpendicular to ***d*** and the four corner vertices (North west, North east, South west, South east) are identified and is discussed below.

3.3.1 Identification of Corner Vertices

The vertex satisfying equation 3.8 is identified as the North East vertex (V_{NE}) and the vertex satisfying equation 3.9 is identified as the South West vertex (V_{SW}) from the set of n vertices defining the parting line.

$$V_{NE}: \quad \max (X_i+Y_i) \quad i=1,2,..,n \tag{3.8}$$

$$V_{SW}: \quad \min (X_i+Y_i) \quad i=1,2,..,n \tag{3.9}$$

Once V_{NE} and V_{SW} have been identified the equation of the straight line segment joining V_{NE} and V_{SW} is used to divide the edges of parting line into two groups. The equation is represented in the form $F(V_{NE} \rightarrow V_{SW})$. If the two vertices of the edge segments defining the parting line satisfies $Y_i \leq F(V_{NE} \rightarrow V_{SW})$ at $X=X_i$ it is identified as E^1 edge group, otherwise it belongs to E^2 edge group as shown in figure 3.14.

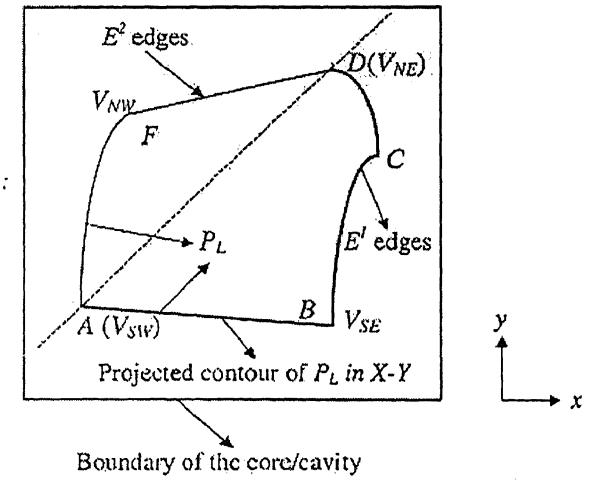

Figure 3.14: Extreme vertices and Edge groups of a parting line.

To obtain V_{NW} and V_{SE}, the mean of x and y coordinates ($\underline{X}$ and $\underline{Y}$) of V_{NE} and V_{SW} are calculated. In the E^1 edge group, the vertex (other than V_{NW} and V_{SE}) satisfying equation 3.10 is identified as V_{SE}. Similarly V_{NW} is obtained from the E^2 edge group if it satisfies equation 3.11.

$$V_{SE}: \quad \max\{|X_i - \underline{X}| + |Y_i - \underline{Y}|\} \text{ from vertices in } E^1 \text{ edge group.} \qquad (3.10)$$

$$V_{NW}: \quad \max\{|X_i - \underline{X}| + |Y_i - \underline{Y}|\} \text{ from vertices in } E^2 \text{ edge group.} \qquad (3.11)$$

3.3.2 Determination of Extruding Direction

The edge segments forming the parting line are grouped based on their position with respect to the four corner edges and a counter-clockwise arrangement (for $+d$ viewable facet side) and clockwise (for $-d$ viewable facet side) is made as shown in figure 3.15. The extruding directions of the parting edges are as follows and are shown in figure 3.16:

$E(V_{SW} \Leftrightarrow V_{SE})$: $-Y$ direction.

$E(V_{SE} \Leftrightarrow V_{NE})$: $+X$ direction.

$E(V_{NE} \Leftrightarrow V_{NW})$: $+Y$ direction.

$E(V_{NW} \Leftrightarrow V_{SW})$: $-X$ direction.

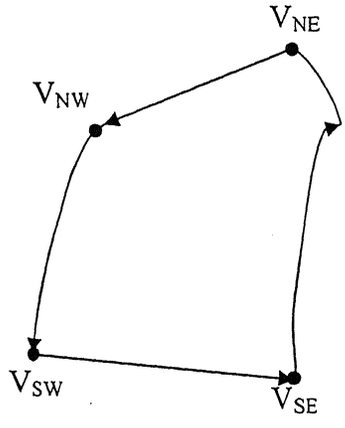

Figure 3.15: Directional arrangement of edges for $+d$ visible facet side

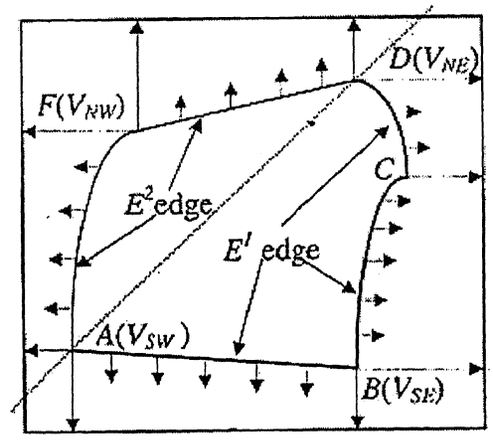

Figure 3.16: Determination of extruding direction

3.3.3 Generation of Parting Surfaces

Once the extruding direction and edge groups are determined the STL file of the parting surface is generated. In the work of Fu et al. [2001], STL file of the parting surface is not generated. Instead a trimmed B-surface is generated. For each edge a planar surface is generated consisting of two coplanar triangles as shown in figure 3.17. The corner points of each group are extruded to generate a single triangle as shown in figure 3.18.

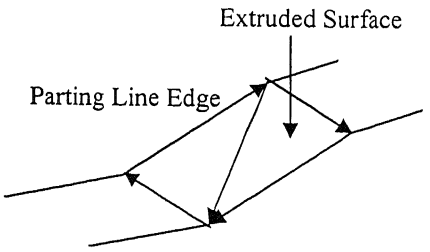

Figure 3.17: Extruded surface of edges

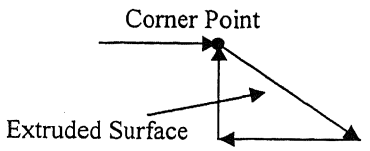

Figure 3.18: Extruded surface of corner points

The X-limits and Y-limits of the parting surface are obtained prior to the extrusion procedure. The x_{max}, x_{min}, y_{max} and y_{min} are obtained from the edge ends of the parting line. The X-limits and Y-limits are then obtained by using equations 3.12 to 3.15.

$$X_{min} = x_{min} - \chi \quad (3.12)$$

$$X_{max} = x_{max} + \chi \quad (3.13)$$

$$Y_{min} = y_{min} - \chi \quad (3.14)$$

$$Y_{max} = y_{max} + \chi \quad (3.15)$$

The value of χ can be taken as input from the user and it determines the extent of offsetting of the parting line to obtain the parting surface.

An example showing the methodology to obtain the coordinates and outward normals of the triangular patches of $+d$ viewable facet side is given below. The edge group from $V_{SW} \Leftrightarrow V_{SE}$ is considered as shown in fig 3.19.

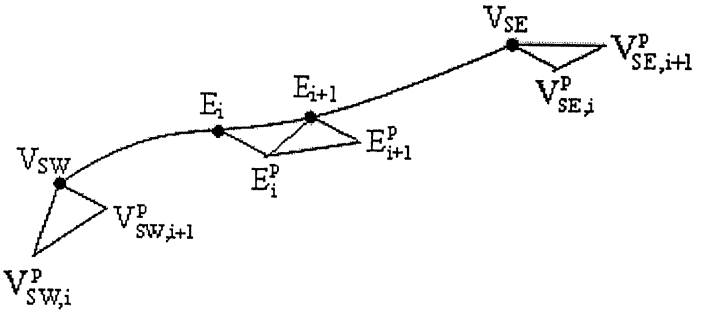

Figure 3.19: Example of extrusion $V_{SW} \Leftrightarrow V_{SE}$

The vertices E_i^p and E_{i+1}^p are obtained by extruding the vertices E_i and E_{i+1} of any edge from $V_{SW} \Leftrightarrow V_{SE}$. Equations 3.16 to 3.21 are used for this purpose.

$$E_i^p(x) = E_i(x) \quad (3.16)$$

$$E_i^p(y) = Y_{min} \quad (3.17)$$

$$E_i^p(z) = E_i(z) \quad (3.18)$$

$$E_{i+1}^p(x) = E_{i+1}(x) \quad (3.19)$$

$$E_{i+1}^p(y) = Y_{min} \quad (3.20)$$

$$E_{i+1}^p(z) = E_{i+1}(z) \quad (3.21)$$

The outward normals η of the two triangular patches can be obtained from equation 3.22.

$$\eta = (E_i^p - E_{i+1}^p) \times (E_i - E_i^p) \quad (3.22)$$

The two corner vertices are also extruded. The coordinates of the end points can be obtained from equations 3.23 to 3.28.

For South West Vertex:

$$V_{SW,i+1}^p(x) = V_{SW}(x) \quad (3.23)$$

$$V_{SW,i+1}^p(y) = Y_{min} \quad (3.24)$$

$$V_{SW,i+1}^p(z) = V_{SW}(z) \quad (3.25)$$

$$V_{SW,i}^p(x) = X_{min} \quad (3.26)$$

$$V_{SW,i}^p(y) = Y_{min} \quad (3.27)$$

$$V_{SW,i}^p(z) = V_{SW}(z) \quad (3.28)$$

The normal can be obtained by: $\eta = (V_{SW,i}^p - V_{SW,i+1}^p) \times (V_{SW} - V_{SW,i}^p)$

The coordinates and normals of surface patch for the South East vertex can be obtained by a similar procedure. All the other three edge groups can be similarly extruded. The difference lies only in the direction of extrusion.

Chapter IV

System Design and Implementation

4.1 Introduction

A system is developed for automatic generation of parting directions, parting lines and surfaces for two-piece permanent molds. The system consists of two main programs and they have the following functionalities.

First main program generates a list containing the values of visibility factors, flatness factor, draw depth factor and overall factor (obtained by summing up the individual factor values), side core and cavity directions (section 2.5) and parting lines of each of the parting directions (section 3.2). The STL file of the component to be molded has to be given as input.

The second main program generates the parting surface once the user chooses a parting direction from the output of first main program. The input to the system is the parting line edges and the STL file of the parting surface is the output.

The system is developed using MSVC++ on WINDOWS 2000. A typical Win32 Console Application type of project is selected. The input files must be present in the same directory that of executable files. The outputs are displayed using Mat Lab 6.5.

4.2 Main Program for Determination of Parting Direction, Parting Line and Side core/cavity Directions

The input to this program is the STL file of the component to be molded, generated using any standard solid modeler like AutoCAD or IDEAS. The input file (STL file) must be in the same directory in which the executable file is present. The output of the program consists of:

- The facets of the separated non-convex regions are stored in a file (*non_convex.txt*). The type of region i.e., whether the region is a true-concave or non-true-concave one and the region number is also stored along with it.
- The non-convex region numbers and the corresponding directions providing local accessibility are stored in a file (*local_direcions.txt*).
- The probable parting directions with various factor values (Visibility factors, Draw depth factor, Flatness factor and Overall factor) are stored in a file (*direction_factor.txt*). The user can select the optimal parting direction from this list.

- The probable parting directions and the associated parting line are stored in a file (*parting_line.txt*). The parting line coordinates are with respect to the transformed coordinate system with the probable parting direction (+*d*) forming the +z direction of the transformed coordinate system.
- The probable parting directions and the corresponding side core/cavity directions are stored in a file (*side_directions.txt*).

The flowchart of this module is shown in figure 4.1.

4.3 Main Program for Parting Surface generation

From the factor values associated with the probable parting directions, the optimal parting direction is selected. From the file containing the probable parting directions and parting line coordinates, the coordinates of the parting line segments corresponding to the optimal parting direction is copied and is pasted in the file named "*parting_surface.txt*". This file acts as input to the program generating the parting surface. The STL file of the parting surface is the output of this program.

The flowchart of this module is shown in figure 4.6.

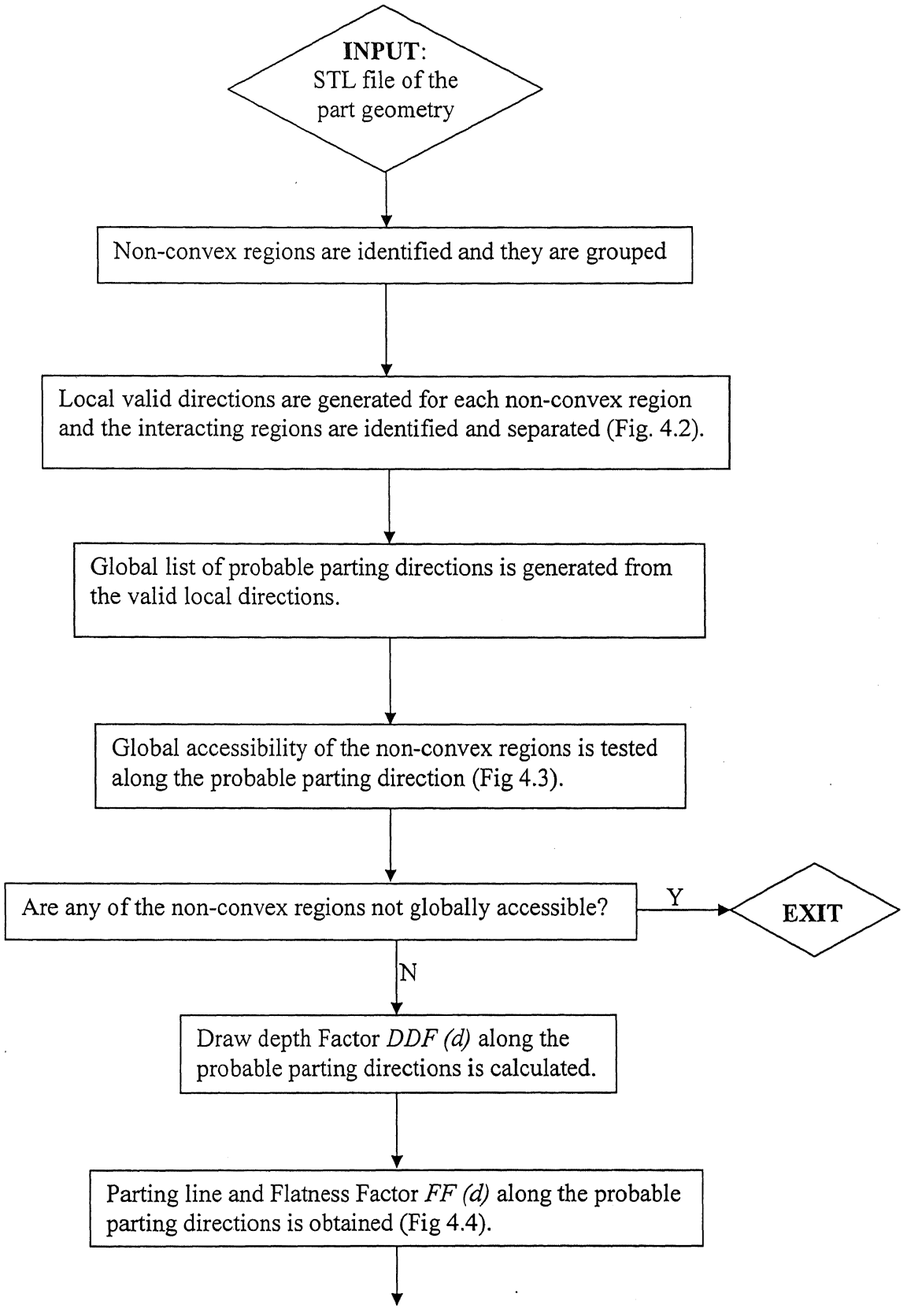
INPUT:
STL file of the part geometry
Non-convex regions are identified and they are grouped
Local valid directions are generated for each non-convex region and the interacting regions are identified and separated (Fig. 4.2).
Global list of probable parting directions is generated from the valid local directions.
Global accessibility of the non-convex regions is tested along the probable parting direction (Fig 4.3).
Are any of the non-convex regions not globally accessible?
Y
EXIT
N
Draw depth Factor DDF (d) along the probable parting directions is calculated.
Parting line and Flatness Factor FF (d) along the probable parting directions is obtained (Fig 4.4).

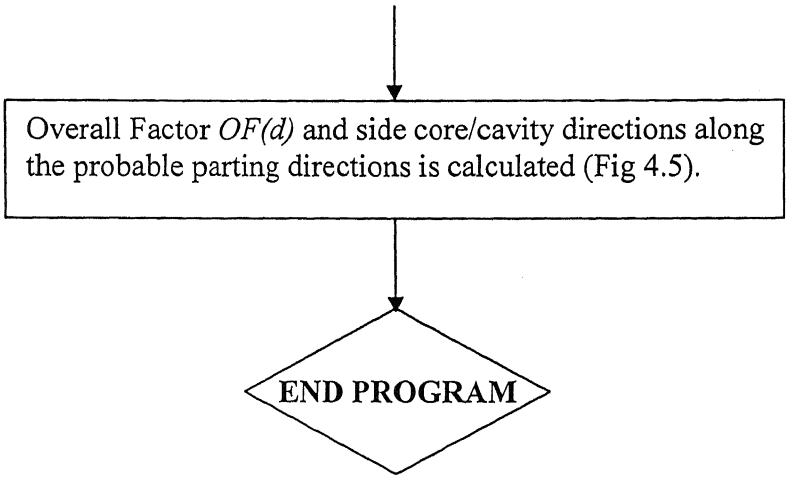

Figure 4.1: Information flow in first main program.

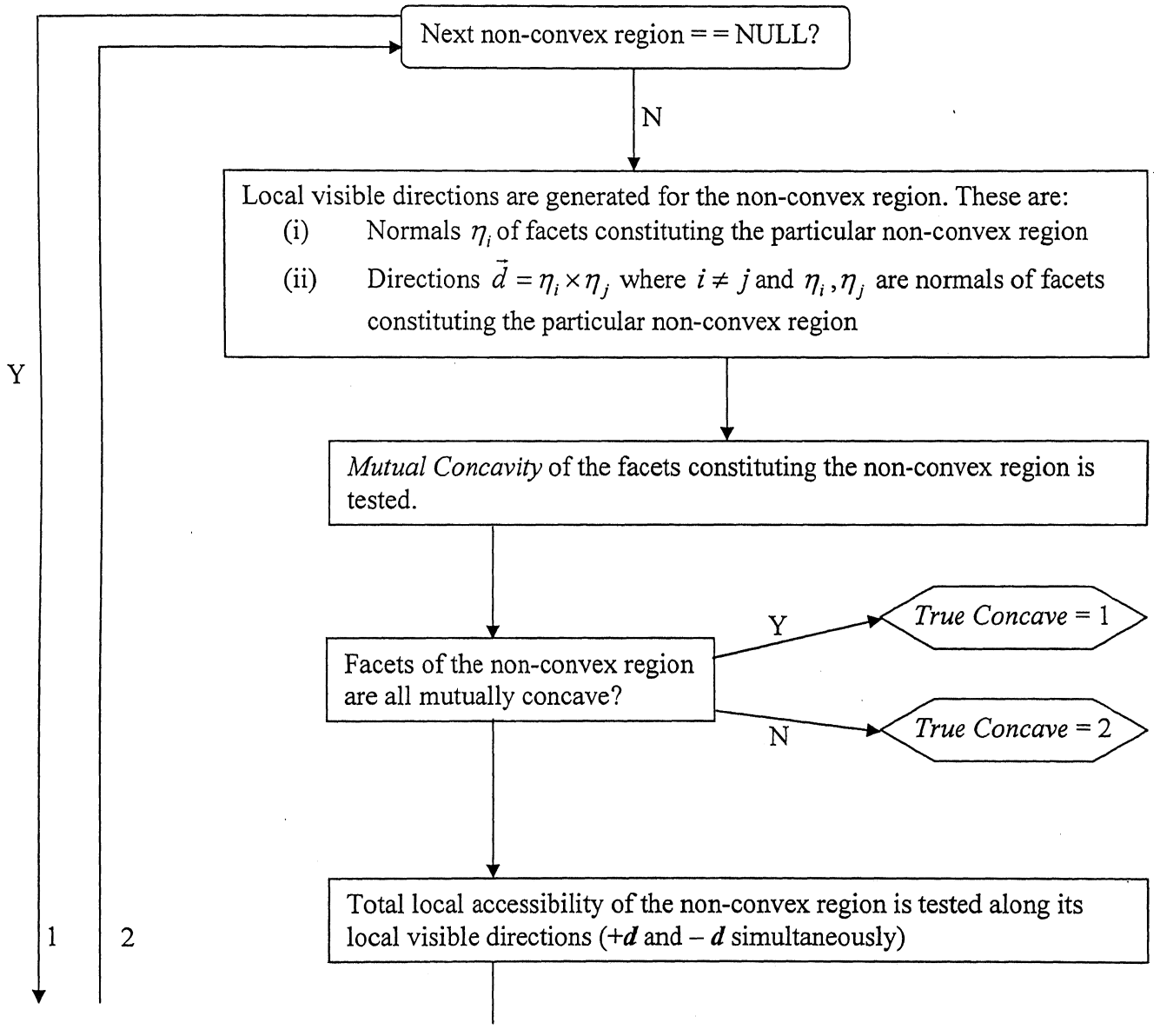

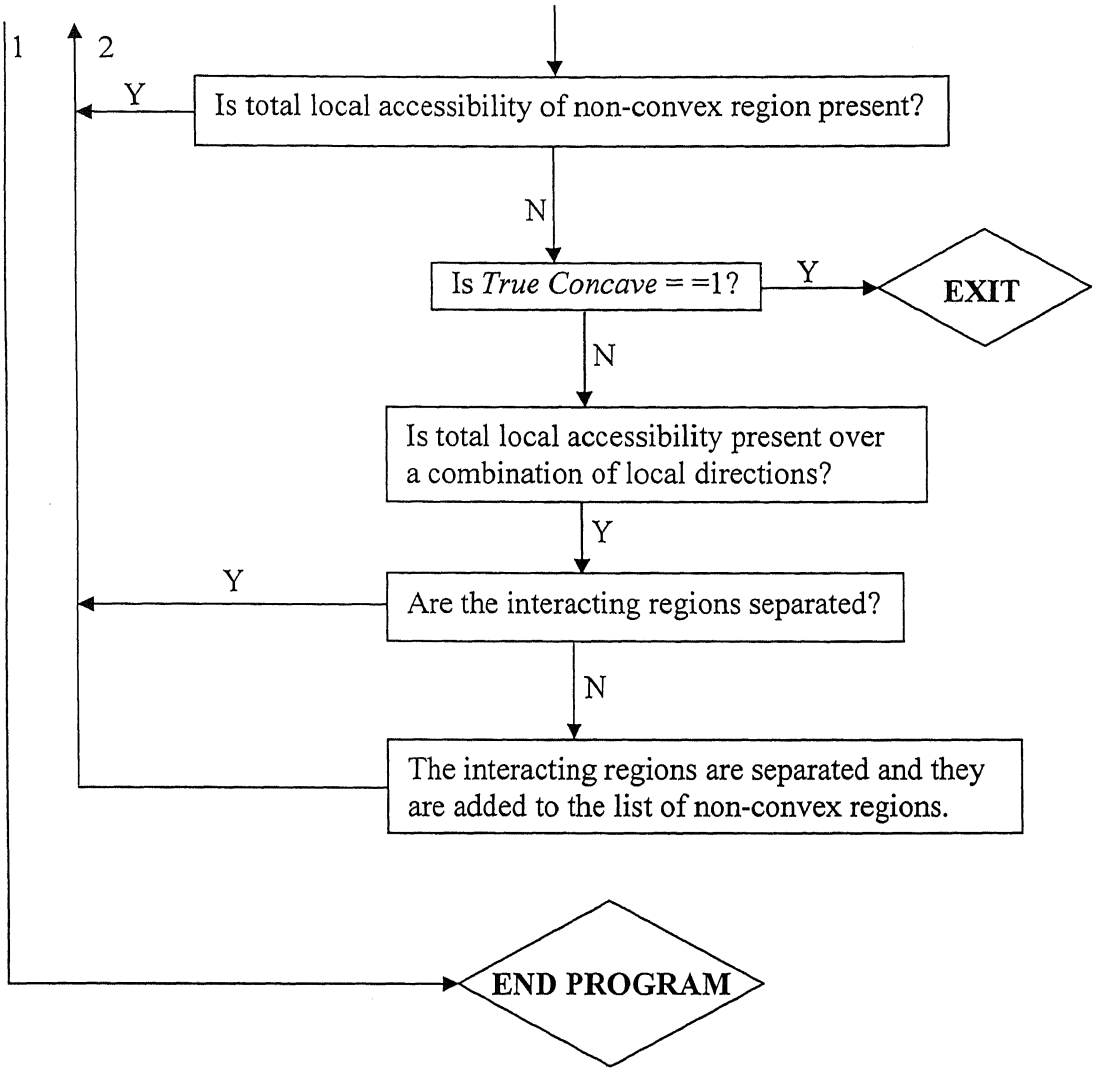

Figure 4.2: Information flow in generation of local valid directions of non-convex regions and identification and separation of interacting regions.

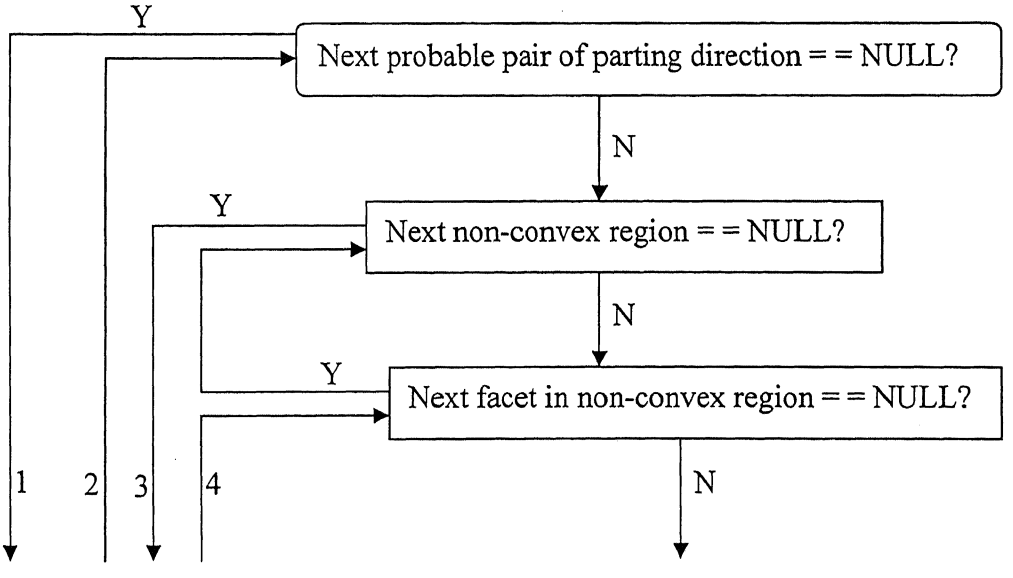

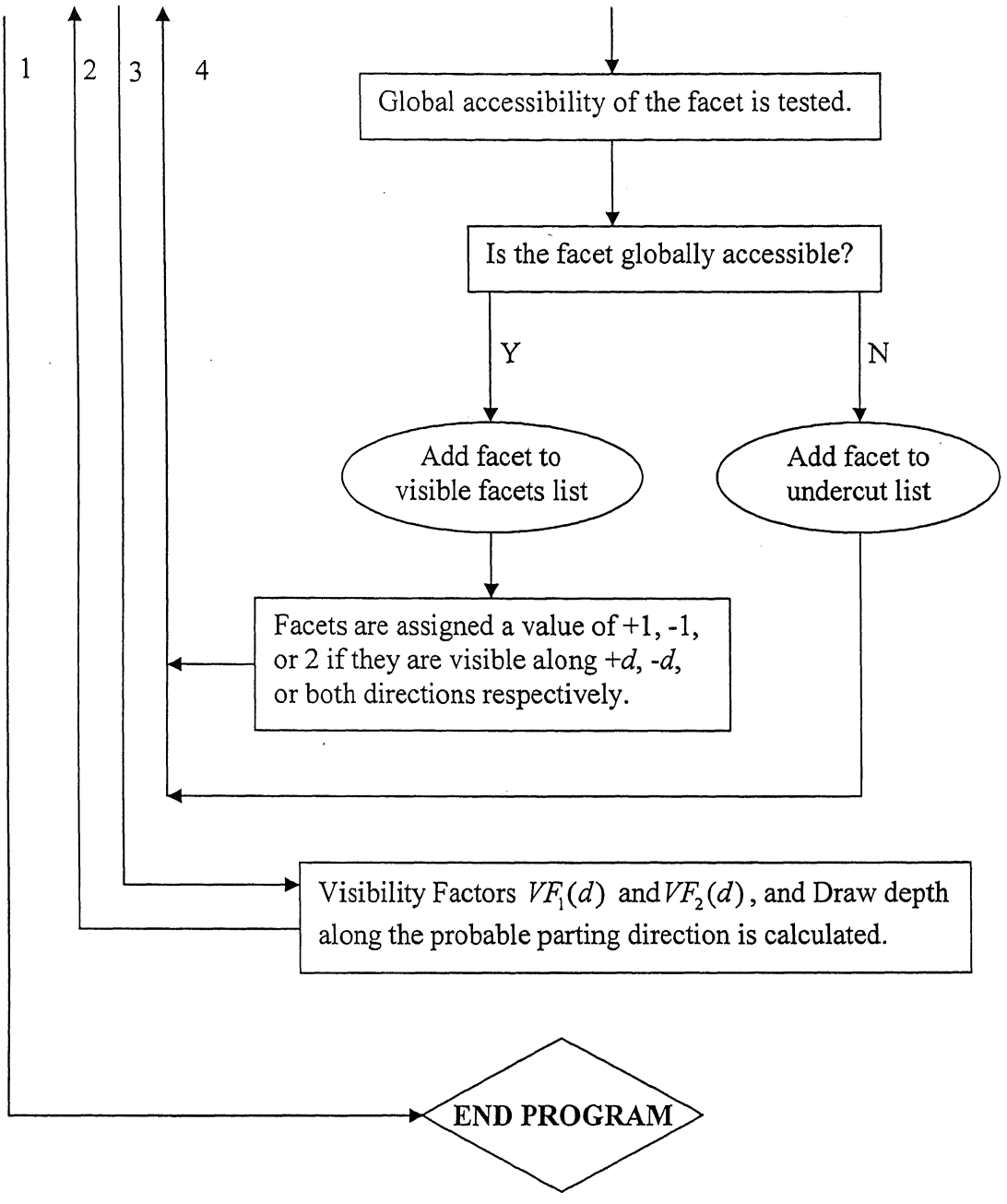

Figure 4.3: Information flow associated with testing of global accessibility of the non-convex regions

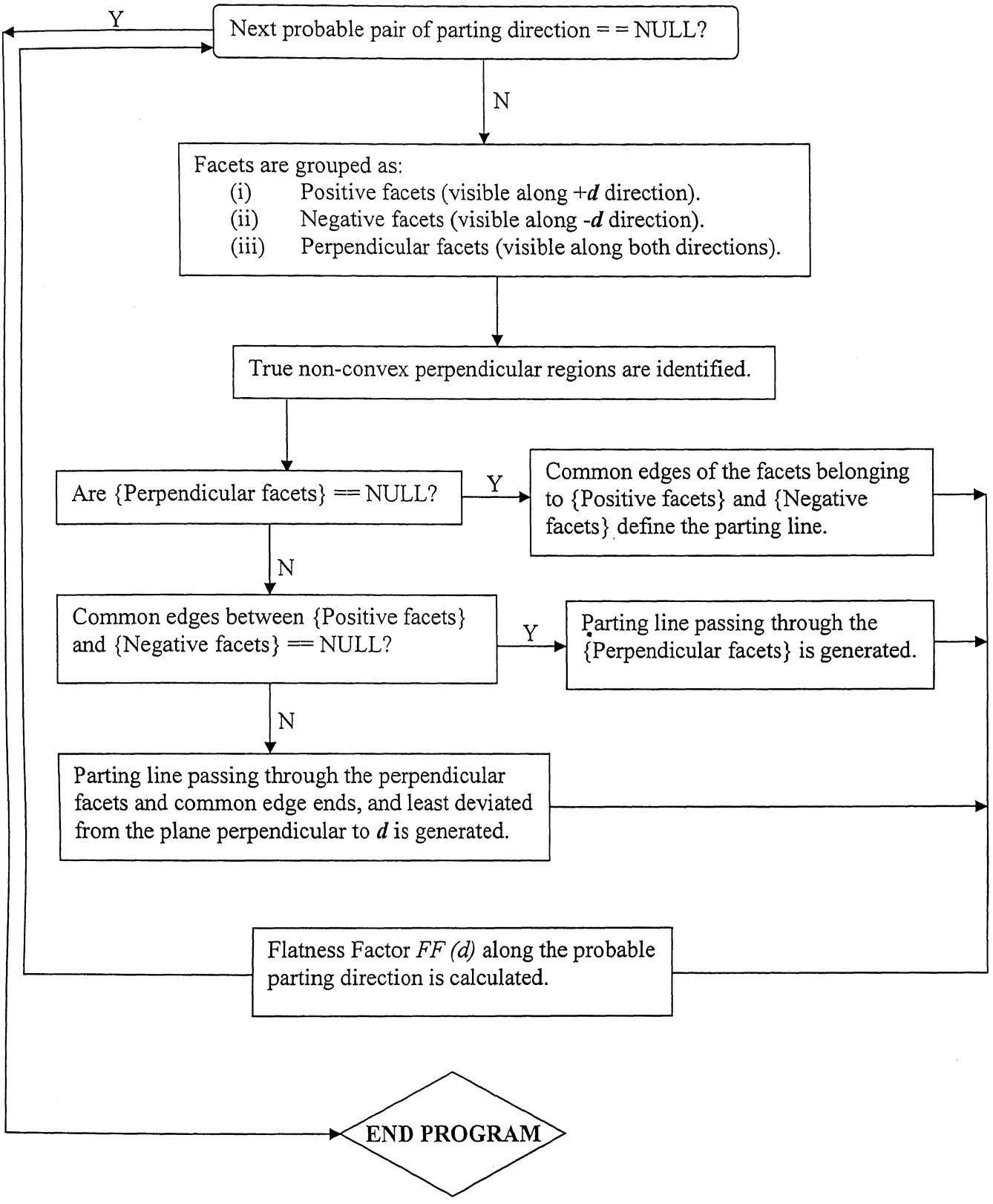

Figure 4.4: Information flow in determination of parting line and flatness factor.

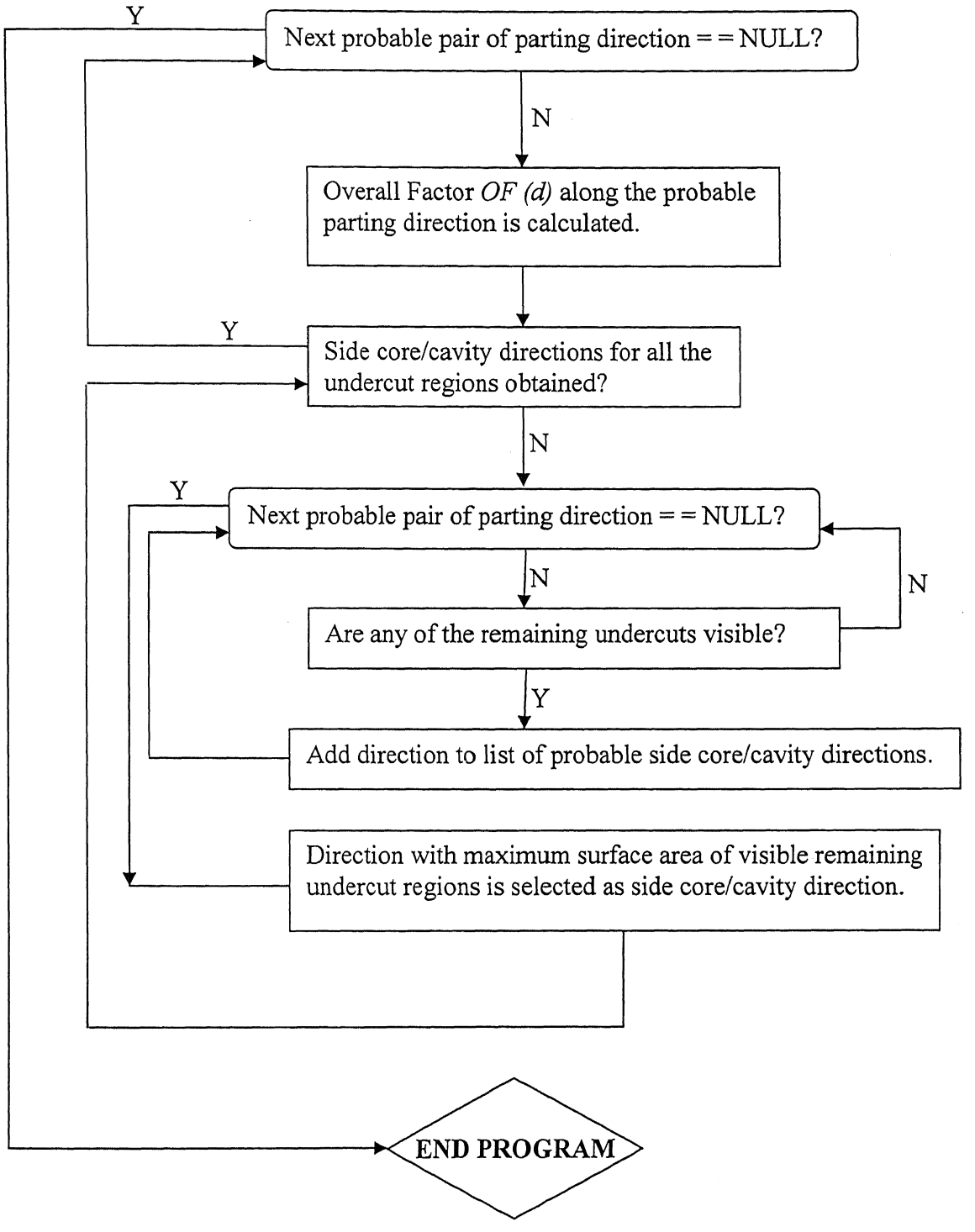

Figure 4.5: Information flow in determination of overall factor and side core/cavity directions.

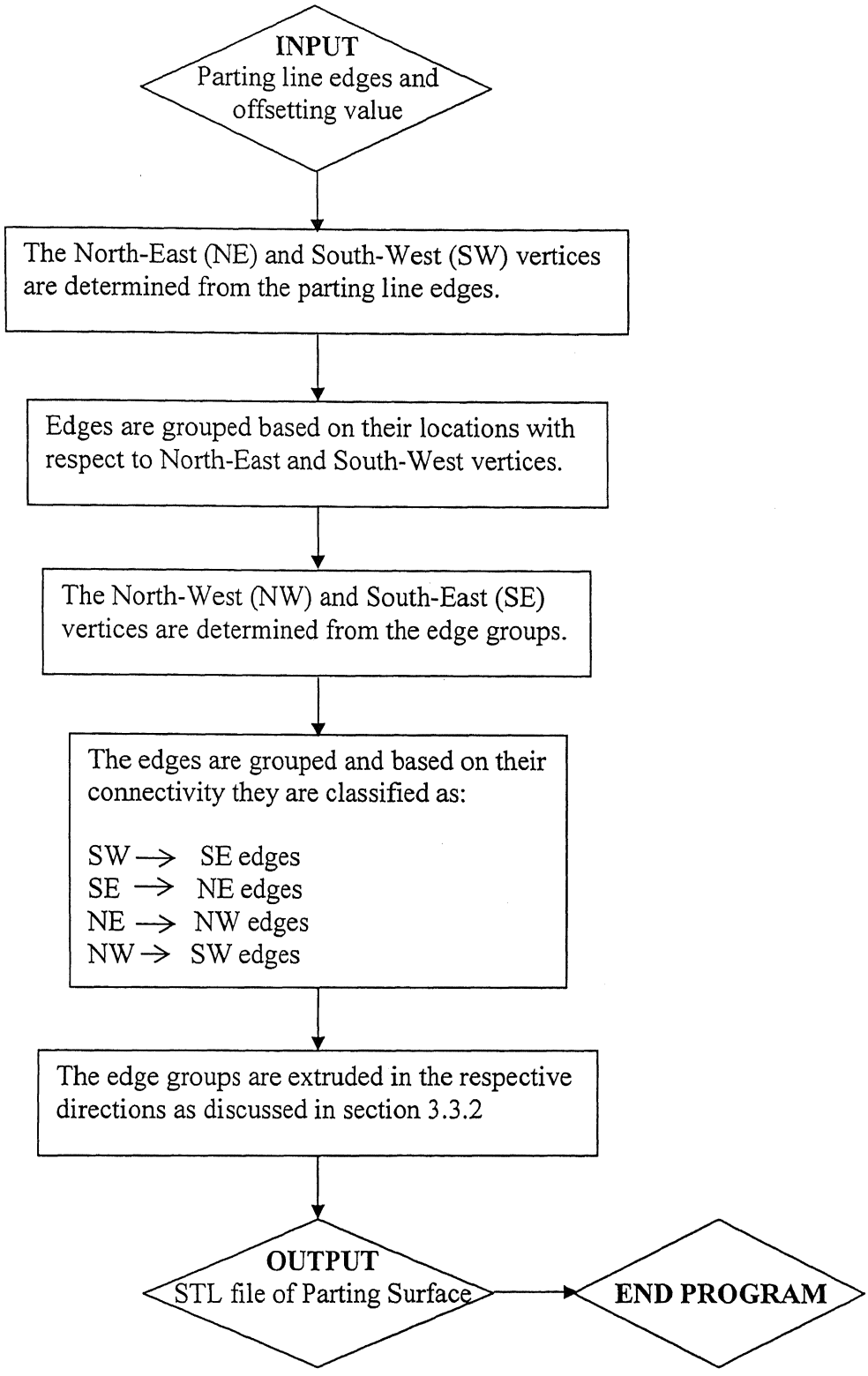

Figure 4.6: Information flow in second main program.

Chapter V

Results and Discussion

5.1 Introduction

An automated system developed during the present work is first validated comparing its predictions with available literature and then few case studies are presented to demonstrate its capabilities. The results of best parting direction and side core/cavity directions based on minimization of surface area and numbers of undercuts is validated with results of Fu et al. [1999] and are presented in section 5.1. The methodology used by Fu et al. [1999] is based on feature recognition and visibility analysis of the features along directions generated based on heuristics. A successful validation establishes the robustness of the system to handle parts involving interacting features. The results of parting line generation are validated with the example given by Weinstein and Manoochehri [1996] and are presented in section 5.2. In most of the previous attempts, parting line along a draw direction is generated by considering the common edges of core and cavity regions. However this may not yield the best parting line as can be inferred from section 3.2. In the methodology developed by Weinstein and Manoochehri [1996] a set of candidate parting lines along a parting direction are generated and the flattest of them is selected as the best parting line. But their methodology can only be applied to parts having planar surfaces. A more generalized methodology is developed and implemented in the present work. Since few attempts [Tan et al., 1990, Weinstein and Manoochehri, 1996, Nee et al., 1998, Fu et al., 2002,] are made on identification and generation of best parting line along a parting direction the example presented by Weinstein and Manoochehri [1996] is selected for validation. Some case studies and the corresponding results are presented in section 5.3. The parts for case studies are so chosen that they contain true-concave as well as non-true-concave regions. The different methodologies developed and implemented in the present work to generate the parting line (section 3.2) are also required while generating the parting lines of the parts.

5.2 Validation

The results of best parting direction and side core/cavity directions based on minimization of surface area and number of undercuts is validated with results of Nee et al. [1999]. The result of best parting line along a direction is validated with the results of Weinstein and Manoochehri [1997].

5.2.1 Best Parting Direction based on minimization of Surface area and Number of Undercuts

A proportional part (Fig 5.1) similar to the one used by Fu et al. [1999] is used to verify the results of the best parting direction based on minimization of surface area and number of undercuts. The isolated non-convex regions are shown in figure 5.2. The best parting direction is selected from the list of draw directions shown in table-5.1. The pair of directions that minimizes the surface area and number of undercuts is selected as the best pair of parting direction. From table-5.1 it can concluded that the direction $0\boldsymbol{i} + 1\boldsymbol{j} + 0\boldsymbol{k}$ is the best parting direction and it matches with the result of Fu et al. [1999]. In the attempt of Fu et al. [1999] the candidate parting direction set is generated heuristically. But in complicated components involving freeform features, such a direction set will not be sufficient enough to yield the optimum parting direction. A more satisfactory result can be obtained by using the present system which has a larger and more complete direction set. The side core/cavity directions for all the probable pair of parting directions are shown in table-5.2.

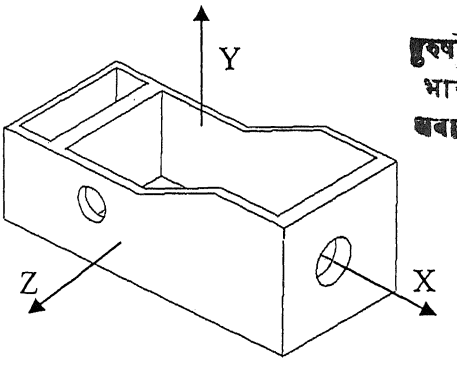

Figure 5.1: An example part similar to that used by Fu et al. [1999].

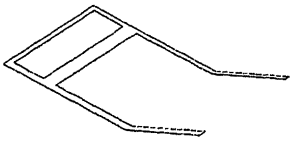

Non-convex region 1

Non-convex region 2

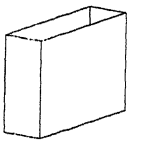

Non-convex region 3

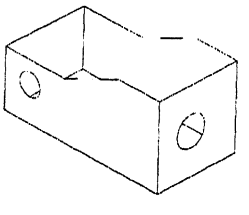

Non-convex region 4

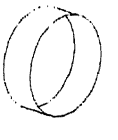

Non-convex region 5

Figure 5.2: Non-convex regions of the part used by Fu et al. [1999]

Table 5.1: Draw directions and the corresponding visible non-convex regions

Draw direction	Total visible area of non-true-concave regions (unit of imported solid model)	Number of visible true-concave regions	Visible region number	Total or partial visibility of the region	Direction of visibility of the region (+***d*** or – ***d*** or both)
$0\boldsymbol{i} + 0\boldsymbol{j} + 1\boldsymbol{k}$ 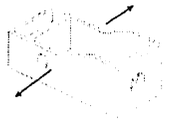	0	2	1	1 (total)	2 (both)
			2	1 (total)	1 (+***d***)
$1\boldsymbol{i} + 0\boldsymbol{j} + 0\boldsymbol{k}$ 	0	2	1	1 (total)	-1 (-***d***)
			5	1 (total)	1 (+***d***)
$0\boldsymbol{i} + 1\boldsymbol{j} + 0\boldsymbol{k}$ 	0	3	1	1 (total)	1 (+***d***)
			3	1 (total)	1 (+***d***)
			4	1 (total)	1 (+***d***)
$-0.400832\,\boldsymbol{i} + 0.916152\,\boldsymbol{j} + 0\boldsymbol{k}$ 	0	1	1	1 (total)	1 (+***d***)

Table 5.2: Draw directions and the corresponding side core/cavity directions

Draw direction	Side core/cavity directions	Visible region number	Direction of visibility of the region (+*d* or –*d* or both)
$0i + 0j + 1k$ 	$1i + 0j + 0k$	5	1 (+*d*)
	$0i + 1j + 0k$	3	1 (+*d*)
		4	1 (+*d*)
$1i + 0j + 0k$ 	$0i + 0j + 1k$	2	1 (+*d*)
	$0i + 1j + 0k$	3	1 (+*d*)
		4	1 (+*d*)
$0i + 1j + 0k$ 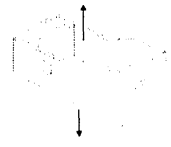	$0i + 0j + 1k$	2	1 (+*d*)
	$1i + 0j + 0k$	5	1 (+*d*)
$-0.400832\,i + 0.916152\,j + 0k$ 	$0i + 0j + 1k$	2	1 (+*d*)
	$1i + 0j + 0k$	5	1 (+*d*)
	$0i + 1j + 0k$	3	1 (+*d*)
		4	1 (+*d*)

5.2.2 Best Parting Line

The results of parting line generation are validated with the example of Weinstein and Manoochehri [1996] (Fig 5.3). In their methodology six candidate parting lines were generated along the draw direction ($0i + 1j + 0k$) and the best parting line was selected from the list of candidate parting lines. The major drawback of their methodology, discussed in section 1.2.2, is that it can obtain parting lines only along those directions which have no undercut and for parts having planar surfaces. Moreover, their methodology do not guarantee flattest parting line along a direction The methodology developed in the present work is capable of handling non-planar surfaces and

guarantees the flattest parting line along a direction. The present methodology can also generate parting line along directions having undercuts. The best parting line generated along $0\boldsymbol{i} + 1\boldsymbol{j} + 0\boldsymbol{k}$ by the present system is shown in figure 5.4 (displayed using Mat Lab 6.5) and it agrees with the result of Weinstein and Manoochehri [1996].

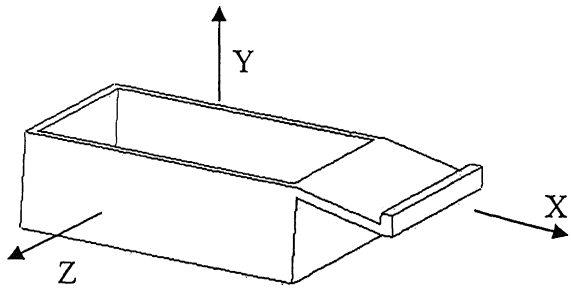

Figure 5.3: Example part used by Weinstein and Manoochehri [1996]

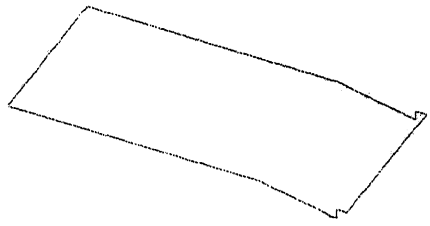

Figure 5.4: Best Parting line along $0\boldsymbol{i} + 1\boldsymbol{j} + 0\boldsymbol{k}$ for the example part shown above

5.3 Case Studies

In the present work, two cases are considered to demonstrate the capabilities of the developed system. The components are fairly simple but all the methodologies developed and implemented in the present system are required to obtain the best parting direction, parting lines and side core/cavity directions. The first component consists of true-concave regions only. The second component consists of true-concave as well as non- true-concave regions. From the results of case studies (section 5.3.1 and 5.3.2) it can be concluded that cumulative influence of the factors (section 2.5) is essential to select the best parting direction. The parting lines obtained in the two case studies demonstrates the competence of the developed methodology to obtain the flattest parting line along a parting direction.

5.3.1 Case I

The capabilities of the present system are demonstrated using the component shown in figure 5.5. The isolated non-convex regions (all true-concave) are shown in figure 5.6. The draw directions and the corresponding visible non-convex regions are shown in table-5.3. The side core/cavity directions for the draw directions are shown in table-5.4.

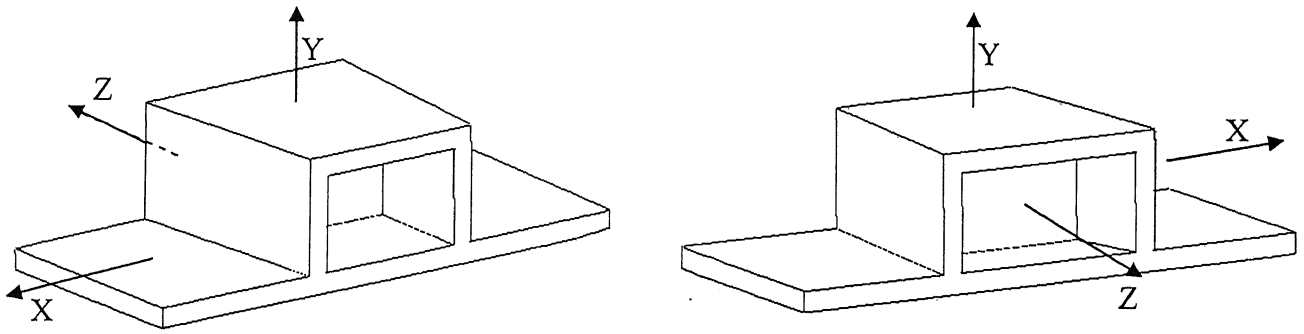

Figure 5.5: Example part used

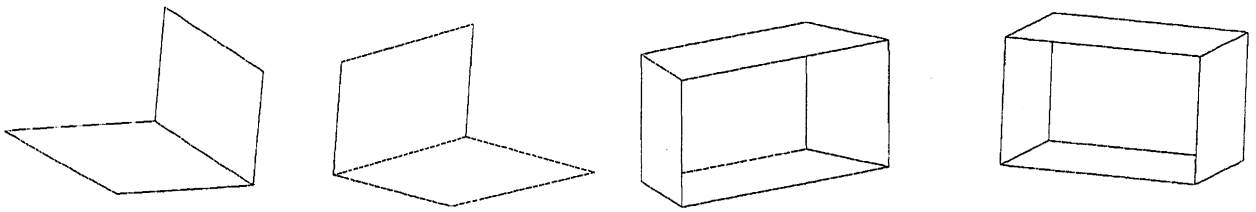

Non-convex region 1 Non-convex region 2 Non-convex region 3 Non-convex region 4

Figure 5.6: Non-convex regions of the part used.

Table 5.3: Draw directions and the corresponding visible non-convex regions

Draw direction	Total visible area of non-true-concave regions (unit of imported solid model)	Number of visible true-concave regions	Visible region number (as given in fig.)	Total or partial visibility of the region	Direction of visibility of the region (+*d* or – *d* or both)
$0i + 0j + 1k$ 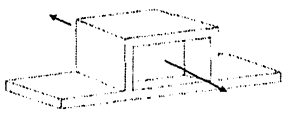	0	4	1	1 (total)	2 (both)
			2	1 (total)	2 (both)
			3	1 (total)	1 (+*d*)
			4	1 (total)	-1 (-*d*)
$1i + 0j + 0k$ 	0	2	1	1 (total)	-1 (-*d*)
			2	1 (total)	1 (+*d*)
$0i + 1j + 0k$ 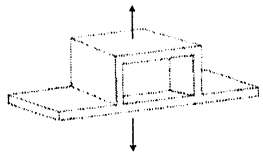	0	2	1	1 (total)	1 (+*d*)
			2	1 (total)	1 (+*d*)
$0.242536\,i + 1j + 0.970142\,k$ 	0	3	1	1 (total)	2 (both)
			2	1 (total)	1 (+*d*)
			3	1 (total)	1 (+*d*)
$-0.242536\,i + 1j + 0.970142\,k$ 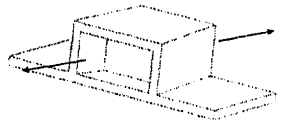	0	3	1	1 (total)	1 (+*d*)
			2	1 (total)	2 (both)
			3	1 (total)	1 (+*d*)

Table 5.4: Draw directions and the corresponding side core/cavity directions

Draw direction	Side core/cavity directions	Visible region number	Direction of visibility of the region (+*d* or –*d* or both)
$0i + 0j + 1k$ 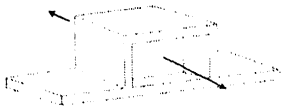	–	–	–
$1i + 0j + 0k$ 	$0i + 0j + 1k$	3	1 (+*d*)
		4	- 1(-*d*)
$0i + 1j + 0k$ 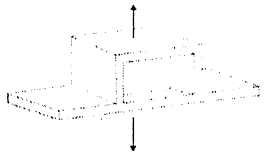	$0i + 0j + 1k$	3	1 (+*d*)
		4	- 1(-*d*)
$0.242536\,i + 1j + 0.970142\,k$ 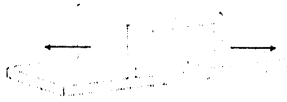	$0i + 0j + 1k$	4	- 1(-*d*)
$-0.242536\,i + 1j + 0.970142\,k$ 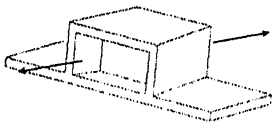	$0i + 0j + 1k$	4	- 1(-*d*)

Best parting lines associated with some of the directions are shown in table-5.5. These parting lines are generated by implementing the methodology described in section 3.2.3 and are displayed using Mat Lab. The factor values along the candidate parting directions are shown in table 5.6. From the table it can be clearly seen that $0i + 0j + 1k$ is the best parting direction. The user can select parting direction can be selected from the candidate parting directions by considering the weighted contribution of the factor-values instead of simple summation of the factor values. In the results shown equal weightages are given to the factor values to determine the best parting direction. However, the user can assign different weightages to the factor values to obtain the best parting direction suitable to him from the list of candidate parting directions

Table 5.5: Draw directions and the corresponding best parting lines

Drawing directions	Best Parting line
$0i + 0j + 1k$ 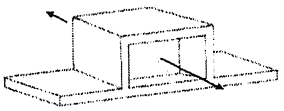	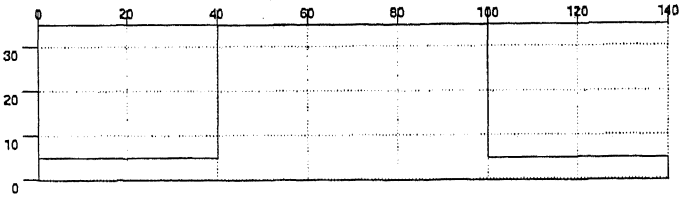
$1i + 0j + 0k$ 	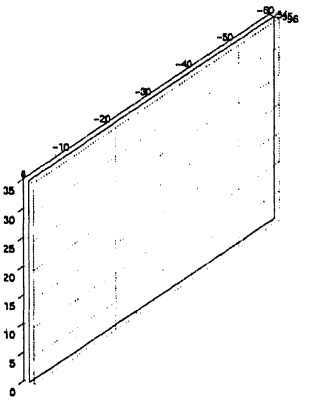
$0i + 1j + 0k$ 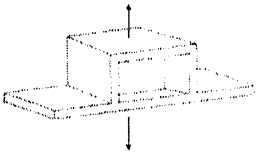	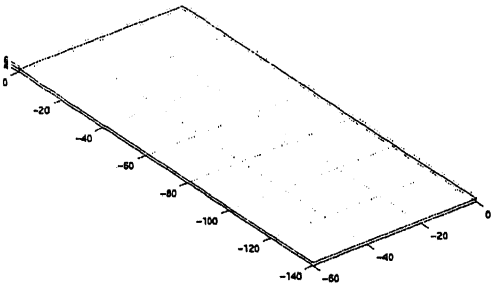
$0.242536\,i + 1j + 0.970142\,k$ 	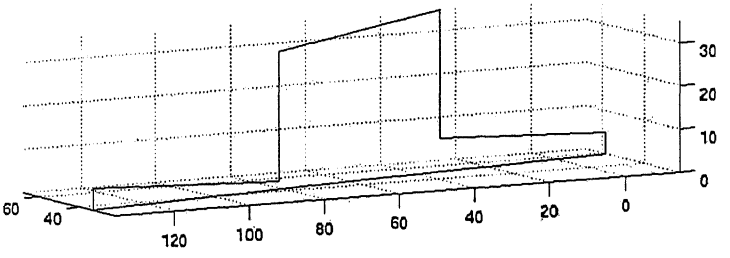

-0.242536 i + 1j + 0.970142 k 	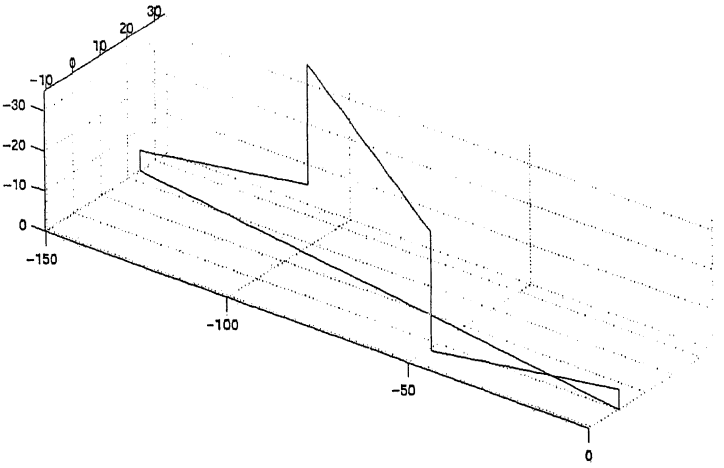

Table 5.6: Draw directions and the corresponding factors

Draw directions	Visibility factor (VF1)	Visibility factor (VF1)	Flatness factor (FF)	Draw depth factor (DDF)	Overall factor (OF)
$0i + 0j + 1k$ 	1	_	1.0	0.571429	2.571429
$1i + 0j + 0k$ 	0.5	_	1.0	0.0	1.5
$0i + 1j + 0k$ 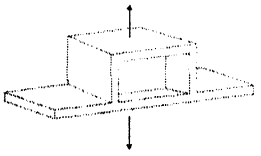	0.5	_	1.0	0.75	2.25
0.242536 i + 1j + 0.970142 k 	0.75	_	0.949208	0.341689	2.040897
-0.242536 i + 1j + 0.970142 k 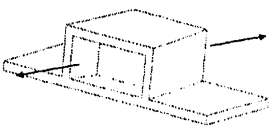	0.75	_	0.940361	0.341689	2.032050

The STL file of the parting surface is generated using the parting line information of the best parting direction. The parting surface generated is shown in figure 5.7 and the procedure is explained in section 3.3. The tessellated surface is shown in figure 5.7(a) and the flat shaded surface is shown in figure 5.7(b).

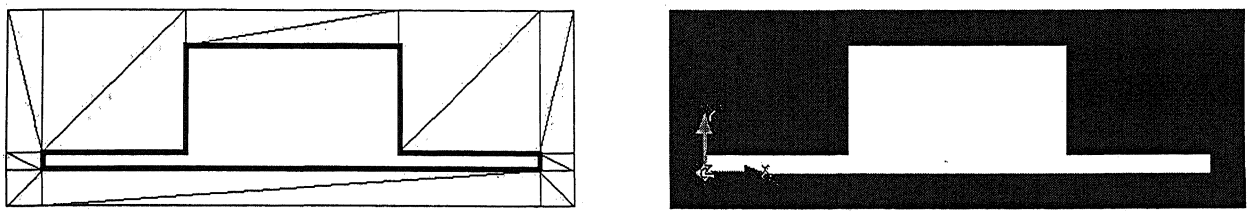

(a) (b)

Figure 5.7: Parting surface generated for the best draw direction.
(a) Tessellated parting surface. (b) Flat-shaded parting surface.

5.3.2 Case II

The capabilities of the present system are demonstrated using the component shown in figure 5.8. The isolated non-convex regions are shown in figure 5.9. The draw directions and the corresponding visible non-convex regions are shown in table-5.7. The side core/cavity directions for the candidate parting directions are shown in table-5.8. Best Parting lines associated with the candidate draw directions are shown in table-5.9. The factor values of the candidate draw directions are shown in table-5.10

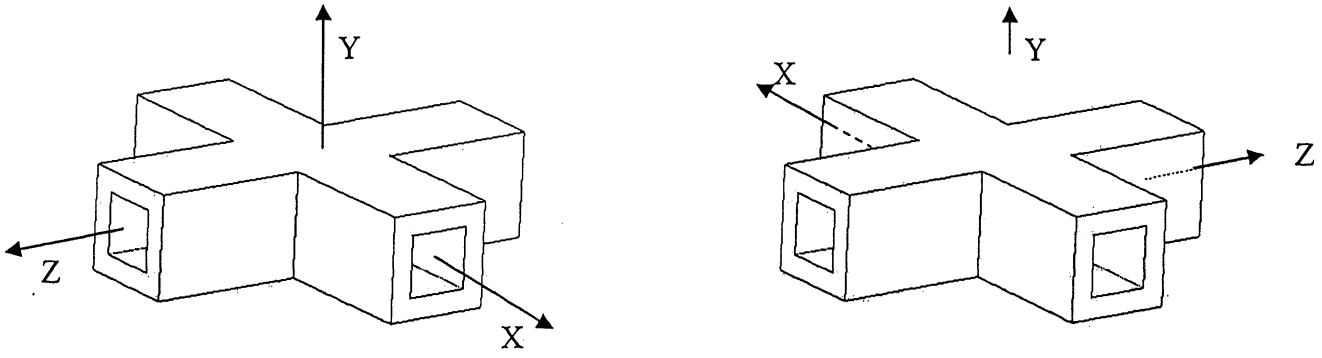

Figure 5.8: Example part used

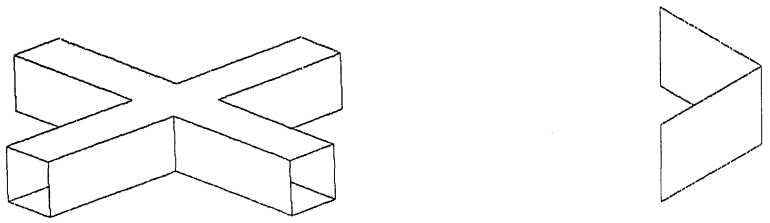

Non-convex Non-convex

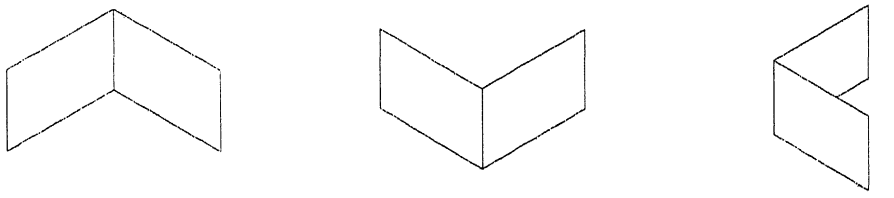

Non-convex Non-convex Non-convex

Figure 5.9: Non-convex regions of the part used.

Table 5.7: Draw directions and the corresponding visible non-convex regions

Draw direction	Total visible area of non-true-concave regions (unit of imported solid model)	Number of visible true-concave regions	Visible region number (as given in fig.)	Total or partial visibility of the region	Direction of visibility of the region (+*d* or –*d* or both)
$0i + 0j + 1k$ 	222	4	1	2 (partial)	0
			2	1 (total)	1 (+*d*)
			3	1 (total)	1 (+*d*)
			4	1 (total)	-1 (-*d*)
			5	1 (total)	-1 (-*d*)
$1i + 0j + 0k$ 	222	4	1	2 (partial)	0
			2	1 (total)	-1 (-*d*)
			3	1 (total)	1 (+*d*)
			4	1 (total)	-1 (-*d*)
			5	1 (total)	1 (+*d*)

$0i + 1j + 0k$ 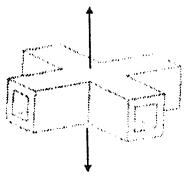	0	2	2	1 (total)	2 (both)
			3	1 (total)	2 (both)
			4	1 (total)	2 (both)
			5	1 (total)	2 (both)

Table 5.8: Draw directions and the corresponding side core/cavity directions

Draw direction	Side core/cavity directions	Visible region number	Direction of visibility of the region (+*d* or –*d* or both)
$0i + 0j + 1k$ 	$1i + 0j + 0k$	1 (rest of the region)	2 (both)
$1i + 0j + 0k$ 	$0i + 0j + 1k$	1 (rest of the region)	2 (both)
$0i + 1j + 0k$ 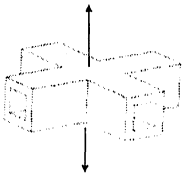	$0i + 0j + 1k$	1 (partial)	2 (both)
	$1i + 0j + 0k$	1 (rest of the region)	2 (both)

Table 5.9: Draw directions and the corresponding parting line

Drawing directions	Best Parting line
$0i + 0j + 1k$ 	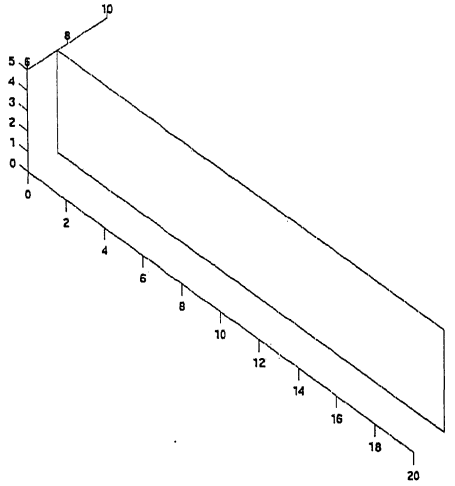
$1i + 0j + 0k$ 	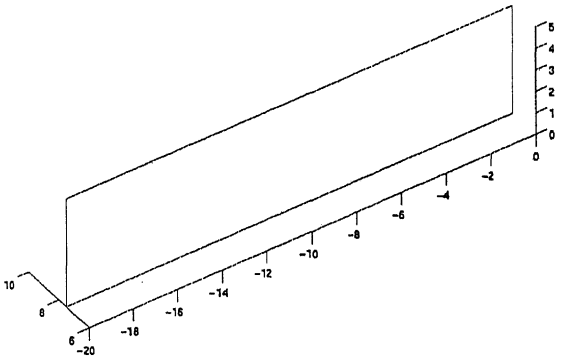
$0i + 1j + 0k$ 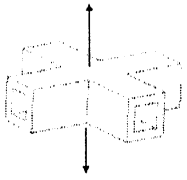	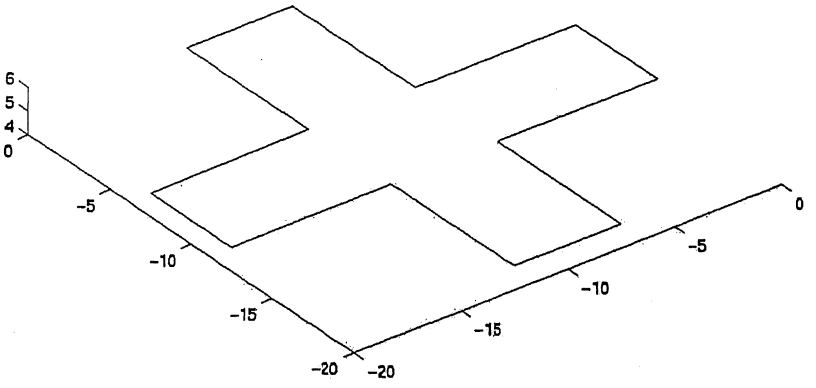

Table 5.10: Draw directions and the corresponding factors

Draw directions	Visibility factor (VF_1)	Visibility factor (VF_2)	Flatness factor (FF)	Draw depth factor (DDF)	Overall factor (OF)
$0i + 0j + 1k$ 	1	0.5	1.0	0.0	2.5
$1i + 0j + 0k$ 	1	0.5	1.0	0.0	2.5
$0i + 1j + 0k$ 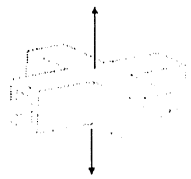	1	0.0	1.0	0.75	2.75

From table-10 it can be concluded that $0i + 1j + 0k$ is the best parting direction. It can be observed that although direction $0i + 1j + 0k$ has greater surface area of undercuts than draw directions $1i + 0j + 0k$ and $0i + 0j + 1k$, still it is the best parting direction because it has appreciably lesser draw depth than the other two directions.

For the valve housing [Gastrow , Injection Molds 102 Proven Designs, Hanser Publishers, Munich Vienna NY, 1983,page: 126-127] shown in figure 5.10, direction having maximum volume and number of undercut is chosen as the main draw direction since it has an appreciably lesser draw depth than the other candidate directions.

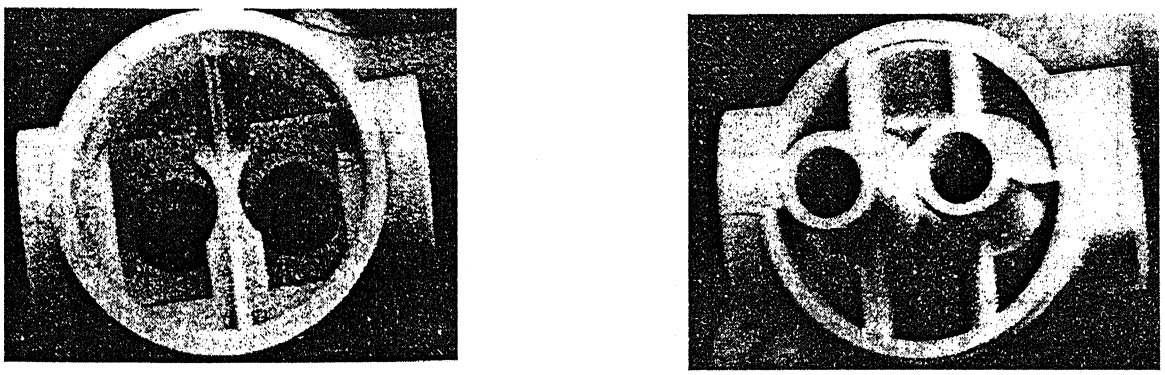

(a) (b)

Figure 5.10: Valve housing [Gastrow, 1983]. (a) View of the interior of the valve housing. (b) View of the exterior of the valve housing.

The STL file of the parting surface is generated from the parting line information of the best parting direction. The parting surface generated is shown in figure 5.11. The tessellated surface is shown in figure 5.11(a) and the flat shaded surface is shown in figure 5.11(b).

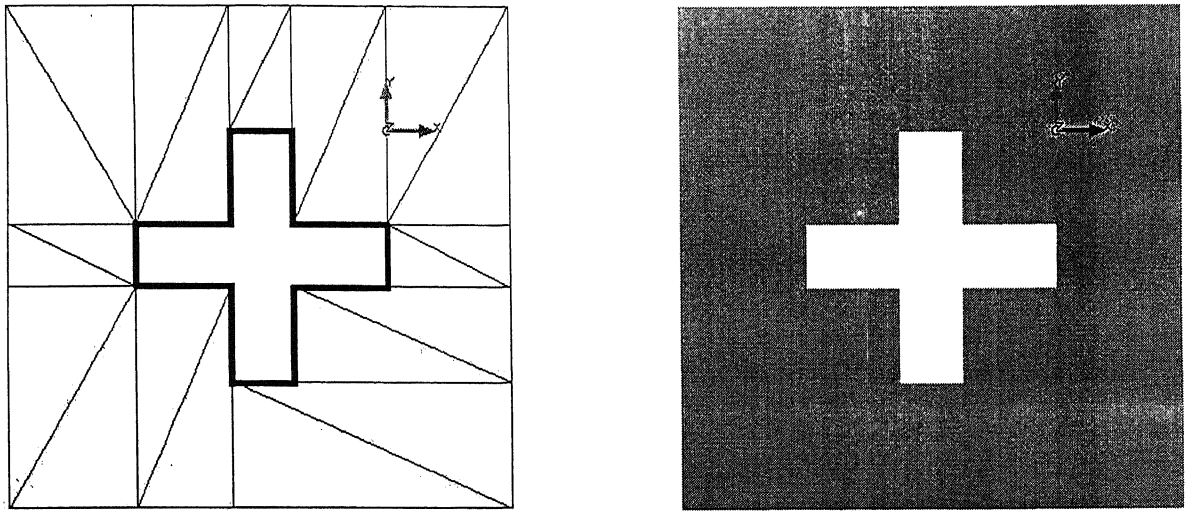

(a) (b)

Figure 5.11: Parting surface generated for the best draw direction.
(a) Tessellated parting surface. (b) Flat-shaded parting surface.

Chapter VI

Conclusion and Scope of Future Work

6.1 Conclusions

The following conclusions are drawn from the present work:

- In the present work a system has been developed that takes STL file of the component (to be injection molded or die casted) as an input and identifies the best pair of parting directions, corresponding side core and cavity directions, generates the parting line and STL file of parting surface.
- The non-convex regions form the probable undercut regions. Hence they are identified and separated. A methodology is developed and implemented whereby interacting non-convex regions are also identified and separated (section 2.2.1.2).
- In the previous attempts, the set of candidate parting directions were generated based on heuristics and were not complete. In the present work, in addition to the set of candidate parting directions used in literature, additional directions are generated (section 2.2). This makes the set of candidate parting directions far more complete.
- The concept of accessibility cone is used while determining the accessible regions along candidate parting directions. Usage of STL file of the part model has a major advantage over B-rep model while determining accessibility since tessellation of the model is made redundant in former case.
- In the previous attempts common edges of core and cavity regions were considered to obtain the parting line along a parting direction. Such a procedure may not guarantee the flattest parting line. Hence a methodology is developed and implemented in the present work to generate the flattest parting line along a parting direction (section 3.2).
- Flatness of parting surface/parting line, surface area and number of undercuts, and draw depth largely influences the productivity, quality and cost of the product manufactured by injection molding or die casting. Hence a cumulative influence of all the three factors is considered while determining the best parting direction.
- A set of candidate parting directions is generated and a quantitative evaluation of each of the factors along each candidate parting direction is carried out to obtain the corresponding factor-values. For each candidate direction the factor-values are added to obtain the overall-factor value. The parting direction having the maximum value of the overall-factor is selected as the best parting direction.

- Once the best parting direction is determined, the STL file of the parting surface is generated by extruding the parting line (section 3.3).

6.2 Scope of Future Work

Further work can be carried out in the determination of optimal parting directions, parting lines and surfaces using the STL file of the component as input and these are as follows:

- Components requiring split cores can be done.
- In the present work a facet is considered to be totally inaccessible even if it is partially inaccessible, i.e. true/absolute accessibility analysis of a facet is not done. Hence absolute accessibility analysis of facets can be carried out. This can help in identifying the regions requiring split cores.
- STL file of the mold halves having the side core/cavity regions, runners, cooling channels etc. can be generated. This can help in manufacturing the mold halves by Rapid Tooling.
- A more accurate determination of draw depth can be carried out.
- The identification of core and cavity sides can be done using G-Map of the non-convex regions.

References

Chen L.L., Chou S.Y., Woo T.C., 1993, Parting directions for mold and die design. Computer Aided Design, 25 (12), 762-768.

Dhaliwal S., Gupta S.K., Huang J., Priyadarshi A.K., 2002, Algorithms for computing global accessibility cones. Technical research report number TR 2002-30. [http://www.isr.umd.edu].

Eberly D., 2003, Intersection of convex objects: The method of separating axes. [http://www.magic-software.com].

Fu M.W., Fuh J.Y.H., Nee A.Y.C., 1999, Undercut feature recognition in an injection mould design system. Computer-Aided Design, 31(12), 777-790.

Fu M.W., Fuh J.Y.H., Nee A.Y.C., 2001, Core and cavity generation method in injection mould design. International Journal of Production Research, 39 (1), 121-138.

Fu M.W., Nee A.Y.C., Fuh J.Y.H., 2002, The application of surface visibility and moldability to parting line generation. Computer-Aided Design, 34, 469-480.

Gastrow, 1983, Injection molds – 102 proven designs. Hanser Publishers, Munich Vienna New York.

Hui K.C., 1997, Geometric aspects of the mouldability of parts. Computer Aided Design, 29 (3), 197-207.

Hui K.C., Tan S.T., 1992, Mould design with sweep operations – a heuristic search approach. Computer- Aided Design, 24 (2), 81-91.

Li C.L., 2002, Application of Catmull-Clark subdivision method in plastic injection mould parting surface design. Proceedings of the Sixth International Conference on Information Visualisation (IV'02).

Majhi J., Gupta P., Janardan R., 1999, Computing a flattest, undercut free parting line for a convex polyhedron, with application to mold design. Computational Geometry, 13, 229-252.

Nee A.Y.C., Fu M.N., Fuh J.Y.H., Lee K.S., Zhang Y.F., 1997, Determination of optimal parting directions in plastic injection mold design. Annals of CIRP, 46 (1), 429-432.

Nee A.Y.C., Fu M.W., Fuh J.Y.H., Zhang Y.F., 1998, Automatic determination of 3-D parting lines and surfaces in plastic injection mold design. Annals of CIRP, 47 (1), 95-98.

Priyadarshi A.K., Gupta S.K., 2004, Geometric algorithms for automated design of multi-piece permanent molds. Computer-Aided Design, 36, 241-260.

Ravi M, Srinivasan M.N., 1990, Decision criteria for computer-aided parting surface design. Computer-Aided Design, 22 (1), 11-18.

Tan S.T., Yuen M.F., Sze W.S., Kwong K.W., 1990, Parting line and parting surfaces of injection moulded parts. Proceedings of Institution of Mechanical Engineers, 204, 211-223.

Weinstein M., Manoochehri S., 1996, Geometric influence of a molded part on the draw direction range and parting line locations. Journal of Mechanical Design, 118, 29-39.

Weinstein M., Manoochehri S., 1997, Optimum parting line design of molded and cast parts for manufacturability. Journal of Manufacturing Systems, 16(1), 1-12.

Yin Z, Ding H., Li H., Xiong Y., 2004, Geometric moldability analysis by geometric reasoning and fuzzy decision making. Computer-Aided Design, 36 (1), 37-50.

Ying Z., Ding H., Xiong Y., 2001, Virtual prototyping of mould design; geometric mouldability analysis for near-net-shape manufacturing parts by feature recognition and geometric reasoning. Computer-Aided Design, 33 (2), 137-154.

Appendix A
Transformations

To check the visibility along any pair of directions (+***d*** and –***d***), the +***d*** direction is made the +z-axis of the new coordinate system as shown in figure A.1 and corresponding transformation of facet vertices and normals is made.

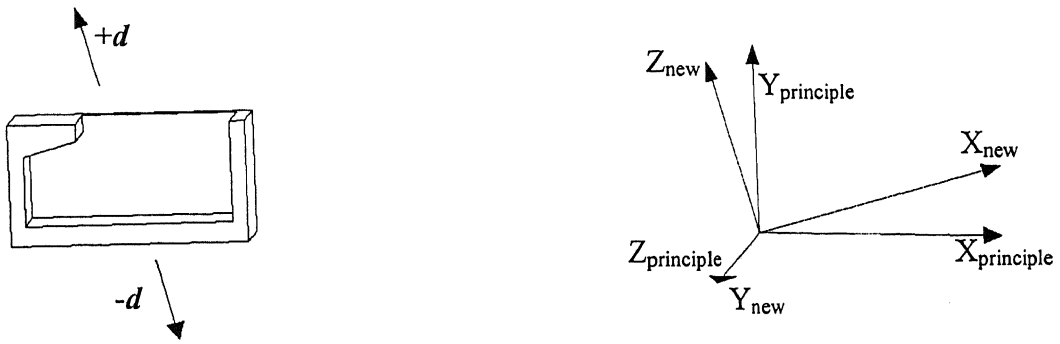

(a) (b)

Figure A.1: One of the probable parting directions and the corresponding new axes system for a part. (a) A part and its probable parting direction are shown. (b) The new axes system corresponding to the probable parting direction.

The x-axis of the transformed coordinate system is obtained from equation A.1.

$$\overline{x}_{new} = \frac{\overline{z}_{principle} \times \overline{z}_{new}}{|\overline{z}_{principle} \times \overline{z}_{new}|} \qquad (A.1)$$

Where $\overline{z}_{principle} = (0 \quad 0 \quad 1)^T$ and $\overline{z}_{new} = (\eta_x \quad \eta_y \quad \eta_z)^T$.

The y-axis must be perpendicular to both $\overline{x}_{new}$ and $\overline{z}_{new}$. It is obtained from equation A.2.

$$\overline{y}_{new} = \overline{z}_{new} \times \overline{x}_{new} \qquad (A.2)$$

If +***d*** is equal to the +z axis of the principle (original) coordinate system then the generation of new coordinate system and transformation is not required.

The direction cosines obtained are as follows:

$$l_1 = -\frac{\eta_y}{\sqrt{\eta_x^2 + \eta_y^2}} \qquad m_1 = \frac{\eta_x}{\sqrt{\eta_x^2 + \eta_y^2}} \qquad n_1 = 0$$

$$l_2 = -\frac{\eta_x \eta_z}{\sqrt{\eta_x^2 + \eta_y^2}} \qquad m_2 = -\frac{\eta_y \eta_z}{\sqrt{\eta_x^2 + \eta_y^2}} \qquad n_2 = \sqrt{\eta_x^2 + \eta_y^2}$$

$$l_3 = \eta_x \qquad m_3 = \eta_y \qquad n_3 = \eta_z$$

The original vertices of a facet are stored in a 3×3 matrix. The transformation shown in equation A.3 is used to generate the coordinates of the vertices with respect to the new coordinate system.

$$\begin{bmatrix} x_1' & x_2' & x_3' \\ y_1' & y_2' & y_3' \\ z_1' & z_2' & z_3' \end{bmatrix} = \begin{bmatrix} l_1 & m_1 & n_1 \\ l_2 & m_2 & n_2 \\ l_3 & m_3 & n_3 \end{bmatrix} \begin{bmatrix} x_1 & x_2 & x_3 \\ y_1 & y_2 & y_3 \\ z_1 & z_2 & z_3 \end{bmatrix} \tag{A.3}$$

The normal of a facet is a free vector. The transformation shown in equation A.4 is used to generate the transformed normal.

$$\begin{Bmatrix} \eta_x' \\ \eta_y' \\ \eta_z' \end{Bmatrix} = \begin{bmatrix} l_1 & m_1 & n_1 \\ l_2 & m_2 & n_2 \\ l_3 & m_3 & n_3 \end{bmatrix} \begin{Bmatrix} \eta_x \\ \eta_y \\ \eta_z \end{Bmatrix} \tag{A.4}$$

Appendix B
Intersection of a line with a plane

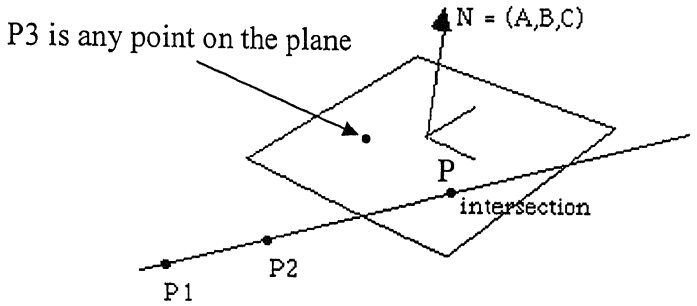

Figure B.1: The intersection of a line and plane.

The equation of a plane (point **P** and point **P3** lying on the plane with normal **N**) can be written as

$$\mathbf{N} \text{ dot } (\mathbf{P} - \mathbf{P3}) = 0 \qquad \text{(B.1)}$$

The equation of the line (point **P** on the line passing through points **P1** and **P2**) can be written as

$$\mathbf{P} = \mathbf{P1} + u\,(\mathbf{P2} - \mathbf{P1}) \qquad \text{(B.2)}$$

If equations B.1 and B.2 are satisfied by point **P** then it is the intersection point of the line (ray) with the plane. This gives equation B.3.

$$\mathbf{N} \text{ dot } (\mathbf{P1} + u\,(\mathbf{P2} - \mathbf{P1})) = \mathbf{N} \text{ dot } \mathbf{P3} \qquad \text{(B.3)}$$

Solving for u gives

$$u = \frac{\mathbf{N} \text{ dot } (\mathbf{P3} - \mathbf{P1})}{\mathbf{N} \text{ dot } (\mathbf{P2} - \mathbf{P1})} \qquad \text{(B.4)}$$

If the denominator of equation B.4 is 0 then the normal to the plane is perpendicular to the line. Thus the line is either parallel to the plane and there are no solutions or the line is on the plane in which case there are an infinite number of solutions

The intersection of the line segment occurs between **P1** and **P2** when u is between 0 and 1.

Appendix C
Method of separating axes

The method of separating axes for 2-D polygons is used to determine whether two stationary convex polygons are intersecting or not. If there exists a line for which the intervals of projection of the two polygons onto that line do not intersect, then the objects do not intersect. Such a line is called a separating line or, more commonly, a separating axis. For a pair of convex polygons in 2D, only a finite set of direction vectors needs to be considered for separation tests. That set includes the normal vectors to the edges of the polygons.

The translation of a separating line is also a separating line, so it is sufficient to consider lines that contain the origin. Given a line containing the origin and with unit–length along direction $\vec{D}$, the projection of a convex polygon C onto the line is the interval shown in equation C.1.

$$I = [\lambda_{\min}(\vec{D}), \lambda_{\max}(\vec{D})] = [\min\{\vec{D} \cdot \vec{X} : \vec{X} \in C\}, \max\{\vec{D} \cdot \vec{X} : \vec{X} \in C\}] \qquad \text{(C.1)}$$

Two convex polygons C0 and C1 are separated if there exists a direction $\vec{D}$ such that the projection intervals I_0 and I_1 do not intersect. Specifically they do not intersect when equation C.2 is satisfied.

$$\lambda^{(0)}_{\min}(\vec{D}) > \lambda^{(1)}_{\max}(\vec{D}) \text{ or } \lambda^{(0)}_{\max}(\vec{D}) < \lambda^{(1)}_{\min}(\vec{D}) \qquad \text{(C.2)}$$

Two nonintersecting polygons that are separated along a direction determined by the normal to an edge of one polygon are shown in fig C.1. Figure C.2 shows two polygons that intersect (there are no separating directions).

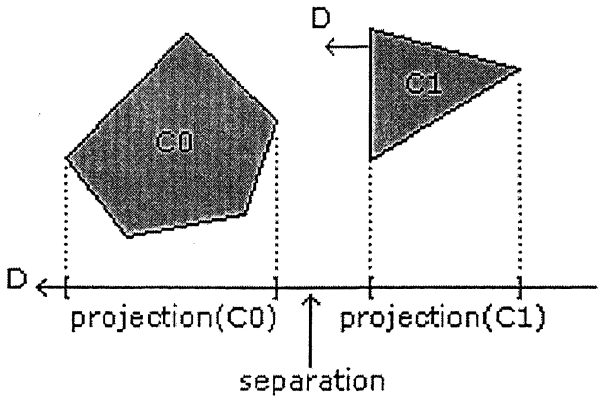

Figure C.1: Figure showing non-intersecting convex polygons

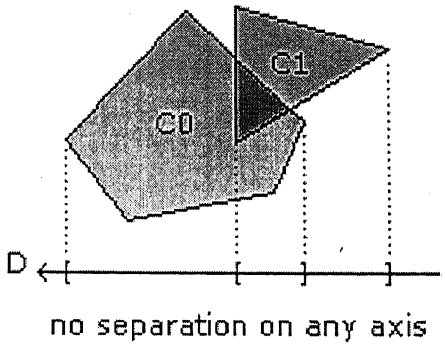

Figure C.2: Figure showing intersecting convex polygons